Nonlinearity 8 (1995) 781–820. Printed in the UK

Three-dimensional model for the formation of longshore sand structures on the continental shelf

Juan Mario Restrepo† and Jerry L Bona‡

† Mathematics and Computer Science Division, Argonne National Laboratory, Argonne, IL 60439, USA

‡ Mathematics Department, The Pennsylvania State University, University Park, PA 16802, USA

Received 2 December 1994, in final form 19 April 1995
Recommended by J D Gibbon

Abstract. A model is proposed for the formation and evolution of three-dimensional sedimentary structures such as longshore sand ridges on the continental shelf in water deeper than that of the shoaling region. Owing to the striking similarity between the bar spacing and the length scales in which interactions among the most energetic modes of shallow water waves take place, we argue that these bars are formed slowly by flows in the turbulent boundary layer generated by weakly nonlinear, dispersive waves. The model is based on the interaction between surficial or internal, weakly nonlinear shallow water waves, having weak spanwise spatial dependence, and the bottom topography. While such underwater structures are not the result of a single formative agent, it is argued that the mechanism proposed in this study does contribute significantly to their generation and evolution.

AMS classification scheme numbers: 86A05, 76B15, 76B25

1. Introduction

The dynamics of sand ridges are not well understood. Sand ridges are underwater barlike features of the continental shelf, composed of loose granular sediment. Hundreds of metres long and up to a few metres high, sand ridges are usually found in groups, arranged in more or less parallel rows separated from each other by hundreds of metres. They may be loosely classified as either tidal ridges or longshore sand ridges. Tidal ridges are oriented more or less parallel to the prevailing direction of the local ocean currents, whereas longshore sand ridges are oriented normal to the direction in which the overlying water waves propagate. In this study we propose a possible mechanism for the formation and evolution of longshore sand ridges.

It deserves emphasis that the often-complex seabed structures appearing off many continental coasts are likely to owe their existence to a multitude of causes. Here we introduce a very simple, wave-generated mechanism that provides a dynamical model of wave-bottom interaction leading to the formation of barlike structures in suitable oceanographic environments. It is not suggested that the intentionally crude model can account for everything we observe. The model is constructed in such a way, however, that it can be implemented using data that is sometimes available from field studies, and without introducing adjustable parameters.

The plan of this paper is as follows. In this introduction, a précis is provided of the morphology of oceanic sedimentary structures; observational and laboratory research in this

0951-7715/95/050781+40$19.50

area is briefly reviewed, and various sedimentation and sandbar models are outlined. The equations describing the evolution of the water waves are covered in section 2. Section 3 deals with the wave-driven boundary layer and with a consequent mass transport equation. To give a qualitative idea of the behaviour of solutions to the model, we present in section 4 several numerical simulations. Section 5 reviews the preceding sections and lists open questions worthy of future pursuit.

1.1. Morphology of oceanic sedimentary structures

Until recently, it was thought that sand ripples, such as those found in the beach zone, and their larger cousins the sandbars and sand ridges were morphologically similar. We now recognize a variety of different sedimentary structures, defining the categories by shape or generating mechanism. Examples are sand ripples, ridge-runnel systems, tidal ridges, and longshore sand ridges.

In the near-beach zone, including the breaker zone, small sand ripples occur on the order of a few centimetres high, which come in a multitude of shapes and forms. Larger structures, such as crescentic bars, occur as well. In this region the fluid flow is quite complex, since there are both incident and reflected waves, tidal flow effects, and turbulence and entrainment of air from wave breaking.

The ridge-runnel system, so common in the near-beach zones in the American Northeast and in the Great Lakes [1], is composed of a large bump 3 to 15 metres away from the beach, about 0.3 metres high and up to perhaps 7 to 10 metres in length, which is preceded by a runnel. The runnel may or may not be scoured with small ripples. The system is thought to be formed by storms eroding the beach and the dune fields and/or by tidal currents [1].

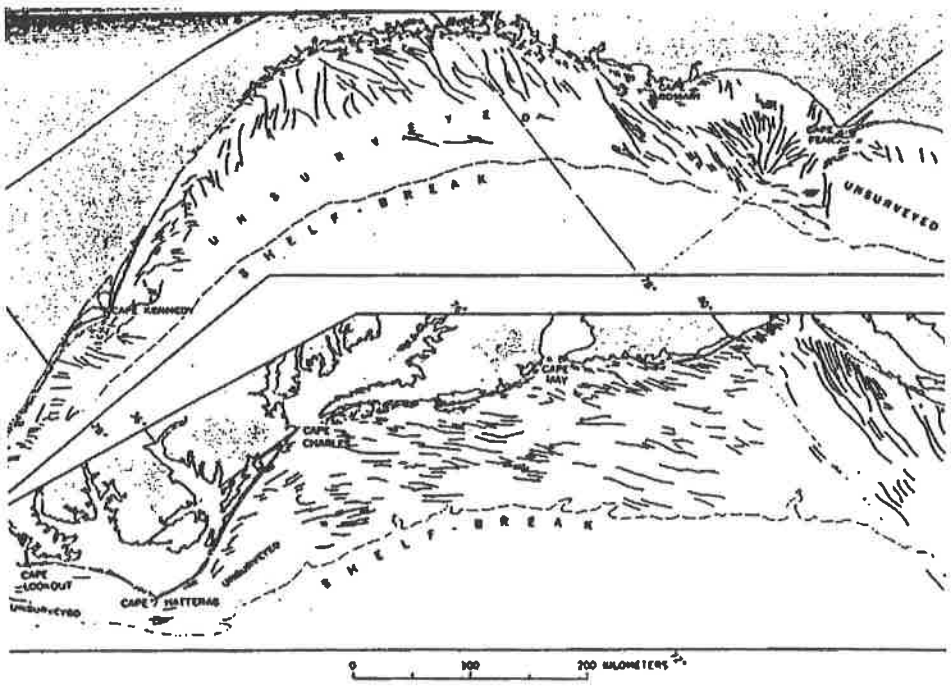

Figure 1. Submerged ridge field from Long Island to Florida, from Swift [4].

Davis *et al* [1] provide observational evidence for their claim that storms seem to play a minor role in the evolution of these structures once they have formed.

Tidal ridges, which were noticed by Off [2], are rhythmic features oriented parallel to the direction of tidal currents. They are 8 to 30 metres high, 7 to 60 kilometres long, and spaced 1 to 10 kilometres apart. Allen [3] found that their height is roughly proportional to the square root of their spacing and that they are composed of sand, silt, and mud. He reported that they occur where tidal currents reach at least 2 to 7 km h^{-1} and where there is an ample supply of sediment. Tidal ridges are also prominent in the neighbourhood of river deltas. Tidal ridges may have a fairly flat dome, suggesting to some researchers that erosion effects play a very minor role.

Sandbars are distributed in complicated patterns on the continental shelf, and it is sometimes difficult to discern which is a tidal ridge and which is a longshore sand ridge, the object of attention in this study. For example, figure 1 taken from a paper by Swift [4] shows the relative orientation of different types of ridges. Note that some bars fan out around river deltas, while some are oriented parallel to or almost normal to the coast.

Longshore sand ridges are common features of the continental shelf in water deeper than the surf zone, from the near-shore region to the farthest reaches of the shelf. The better-known ridge fields are those found in the shallowest end of this range, primarily because they are readily seen, as illustrated in figure 2, which shows the bar system off central Harrison County, Mississippi. Other near-shore systems are found along the coasts of the Carolinas, Florida, the northern coast of Alaska, the Black Sea, the Baltic Sea, and even large lakes such as Lake Michigan. McBride and Moslow [5] trace the origins of many of the sand ridge fields on the inner shelf of eastern North America to ebb and flow delta deposition and the ensuing erosion from tidal flows.

Longshore sand ridges can also be found in the farthest reaches of the shelf hugging every continent around the world. These are the sand ridges of interest to us. Observations suggest that a mean slope in the neighbourhood of 0.02 to 0.05 favours the formation of longshore sand ridges [6]. Such ridges are composed mostly of fine sand and silt, sometimes of mud. The mean sediment particle size ranges between 0.1 and 0.5 millimetres. Groups of up to 12 ridges have been found that are more or less parallel to each other. Some ridge fields are observed to change position over time. Their migration rates vary from place to place; for instance, the ridges on Sable Island Bank have been estimated to move at rates ranging from 0.5 metres per year, in water 60 metres deep, to 5 metres per year, in 30 metre depths [7]. Ridge fields are routinely found in regions where the water depth is small compared with the wavelength of an overlying internal wave environment with frequencies in the infragravity range [8].

It is clear that the formation and maintenance of these sedimentary structures are connected with the ambient hydrodynamics. One possibility is that ridges are generated by major events such as storms, while another prospect is that they come about as a result of systematic aspects of the surrounding fluid flows. Lau and Travis [6] found that sandbars beyond the breaker zone do not disappear but simply change location after a severe storm. Short, in his field observations in northern Alaska [8], found that severe storms seem to rework the bars, but that some sandbars photographed in 1949 and 1955 were still identifiable after approximately thirty years. Preliminary data from the so-called Super Duck [9] experiments show this bar 'reworking' as a consequence of major storms. Other evidence points in the same direction and inclines one to the view that systematic aspects of the hydrodynamic environment play a decisive role in ridge generation. A related question is whether wave breaking is an essential ingredient in the generative processes leading to sand ridges. While categorical evidence does not present itself, sand ripples do form in

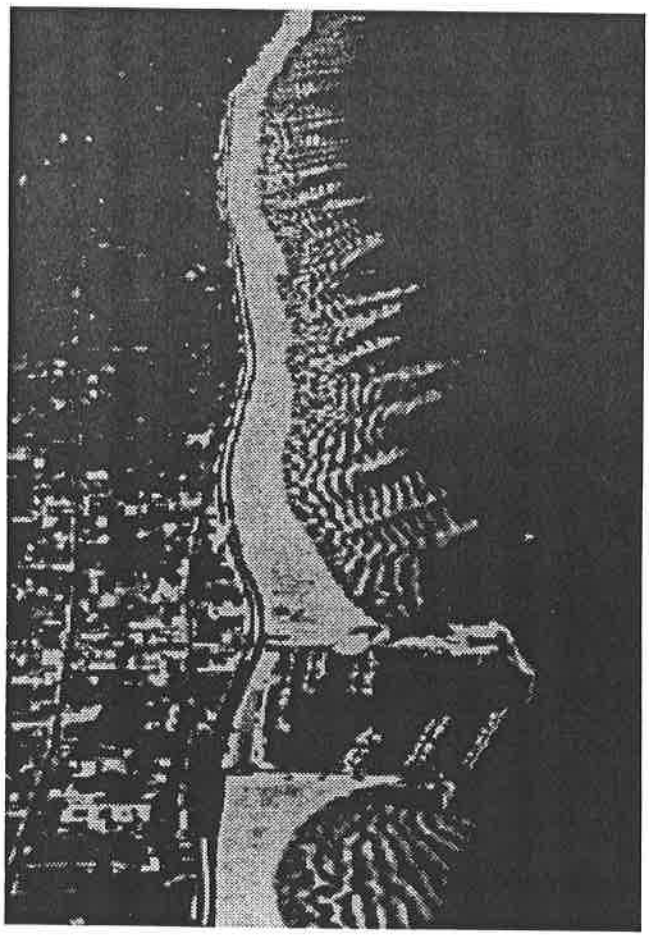

Figure 2. Sand ridges in shallow water, Harrison County, Mississippi.

a laboratory flume under the action of waves; moreover, sand ridges appear in regions where there is no apparent breaking. Both these points will figure in the mathematical conceptualization of the situation presented in this paper.

Several significant differences exist in the near and far ends of the continental shelf insofar as the fluid environment is concerned. First, in the near-shore zone, strong incident and reflected components to the wave field may be identified. Second, the effect of wind stresses on the boundary layer flows is quite significant in the near shore. Third, while significant asymmetry exists in the velocity field in both areas, quite pronounced asymmetry can occur in the acceleration field in the near-shore case. Bijker *et al* [10] made laboratory measurements of acceleration and velocity fields for water waves with fairly high Stokes numbers, in the range of 12–57. They found the net transport to be in the direction of the wave, particularly if the wave was very nonlinear. Smaller particles seemed to be transported mostly by the Stokes flow, whereas larger particles responded in the main to the 'acceleration' field. Hallermeier [11] analysed a large experimental data set and found an empirical rule for the prediction of ripple characteristics based on the acceleration field, which suggests that this field may be an important sand-transport mechanism in the near-beach zone. Elgar *et al* [12] made measurements in the shoaling region, in water depths in the range of 1–6 metres, over a topography with mean slope of 5%, and confirmed in

the field the existence of the velocity and acceleration field asymmetry. They found that the acceleration asymmetry becomes increasingly significant with decreasing water depth. These investigations suggest that the acceleration field becomes ever more important as the distance to the beach decreases; our model would not apply in this area, since the adopted transport equation does not include acceleration effects.

1.2. Sediment-transport models

Much of the work on sedimentation has been aimed at understanding how the sediment particles move, rather than how they form large-scale patterns. Most researchers working on sediment transport assume an outer fluid flow at the edge of a boundary layer and attempt to model sediment motion on the bed and in the boundary layer. Sleath [13] presents a good review of the subject, and we therefore content ourselves with a cursory summary of the various sedimentation models.

A model developed by Bagnold [14] and used by Bailard and Inman [15] assumed that wave-induced oscillatory water motion causes sediment to move back and forth with a net expenditure of energy. Although no net transport results in such an oscillatory flow, the energy dissipation acts to keep the sediment in suspension. Once in suspension, any steady current superimposed on this oscillatory flow will then cause a net transport of the suspended sediment in the direction of the instantaneous total bottom stress. Originally a bed-load model, Bagnold's model has also been applied to suspended-load transport for low Froude number flows. A threshold of motion parameter called the Shield's parameter is incorporated into the model to reflect the fact that a critical amount of energy must be imparted on the bed before transport can occur. Smith [16] and Fredsœ [17] applied this model to the ocean environment. They assumed a constant eddy viscosity and obtained criteria for the onset of instability and ripple formation. Richards [18] used instead a turbulent scale that increases linearly in height from the bed, thus obtaining two modes of instability that yield small- and large-scale ripples, respectively. Bagnold's model has also been used with some success in the near-shore zone, in a version that includes the effect of wind on sediment transport rate [19]. However, Bailard and Inman [15] found that the model did not perform adequately when the waves are not normally incident to the beach.

Another sedimentation model by Raudkivi [20] and by Williams and Kemp [21] attributes the formation of ripples to a chance piling of sediment. This deformation then causes the flow to separate, with subsequent building up of the ripple downstream. They attribute the initial small deformation to the random action of highly turbulent velocities, or 'bursts,' close to the bed.

Last, we mention the model in the Longuett-Higgins paper [22]. In this study he showed how a second-order drift velocity, which was first noted by Stokes [23], develops in the boundary layer from an outer linear oscillatory flow or in the bulk of the fluid through the action of nonlinear waves. This drift velocity is capable of transporting sediment, particularly suspended sediment. A number of people have studied this mechanism; of note are Johns [24], who developed explicit expressions appropriate for the ocean environment and studied the character of the drift velocity and its stability, and Blondeaux [25] and Vittori and Blondeaux [26], who looked at the stability and formation for Froude numbers at which flow separation does not occur. They determined adequate height, spacing, and onset thresholds, by comparison with laboratory experiments. The second of these papers introduced more structure and made a case for the inclusion of nonlinear effects in the flow immediately outside of the boundary layer.

1.3. Sedimentary bar models

Among the researchers who have coupled a sedimentation transport model to an oceanic wave field to look at the process of bar formation in the oceanic environment are Holman and Bowen [27]. They use the fully three-dimensional, linearized water wave equations to compute the drift velocity, which in turn they couple to Bagnold's transport model for suspended load. In particular, they examine the edge-wave case in an effort to compute the formation of crescentic bars in the shoaling region. Bowen [28] has also examined the performance of this model in predicting the spacing of longshore ridges and reports good qualitative agreement with field observations.

Laboratory and field observations indicate that standing wave patterns display a Bragg resonance process with an underlying wavy bottom [29, 30]. In a steady-state situation, the ripples develop a spacing that is roughly half the local average length of the water waves. This first-order theory [29, 31–33] is applicable, in principle, to the near-shore environment, because it relies on the scouring effect of a standing wave pattern. It has been widely studied since it is easily implemented in the laboratory; at one or another time, various researchers have implicated this mechanism as the general reason we observe stable sandbars in the near-shore area.

The ridge and runnel system have been modelled with a variant of Bagnold's transport formula by Dean [19] and deVriend [34]. The extent of the model's success is somewhat difficult to discern, however. Since the undertow and the local bed slope are significant and since the effect of the wind in generating stresses on the surface of the ocean must be taken into account, modelling the formation of runnels is very difficult. Russell and Osorio [35] and Bijker *et al* [36] found that on a sloping beach, the mass transport velocity near the bed was onshore before breaking and offshore after. This effect, which seems to be independent of wave reflection from the beach, may explain why these bar systems are usually found close to the plunge line of breakers.

Huthnance [37] developed a theory for the formation of tidal ridges based on an instability triggered by a small protuberance on the shelf. The ensuing boundary layer develops a bar that is fed by bedload. The resulting steady-state bar is finite in extent and parallel to the assumed, always-present currents. Equilibrium is reached when the supply of sand is exhausted. Huthnance noted that the tops of these ridges are flat rather than rounded, which he claimed dismisses erosion as being the source for the generation of these structures. Huthnance's study does not address the periodic nature of these bars, nor does it suggest a relation between their height and spacing.

Among the first to suggest that infragravity waves may be responsible for longshore sand ridge formation was Suhaida [38]. He did so at a time when few people saw anything fundamentally different about near-shore sandbars where a strong standing-wave field may be present, and bars or ridges far from the beach where little or no standing wave pattern is to be found. Short [8], in field measurements of sand ridges in Alaska, found a loose correlation between the ridge spacing and the average peak infragravity component wavelength.

Lau and Travis [6] derived a drift velocity from a Stokes water-wave field for a bed with constant slope. Their model yields the spacing and the number of ridges from the periodicity of the drift velocity. They made use of the SRIT (slightly resonant interacting triads) approximation developed by Lau and Barcilon [39] and Mei and Ümlüata [31] for weakly nonlinear shallow-water waves to solve approximately for the wave motion.

Boczar-Karakiewicz conducted a number of interesting field and laboratory studies [29, 40]. In the analysis of her findings [41], she combined the hydrodynamic approximation of Lau and Barcilon with the boundary-layer theory of Longuett-Higgins [22]. Exploiting

the large discrepancy between the time-scales relevant to wave propagation and sediment dynamics, these investigators formulated the first evolutionary model for sand ridge formation. A variant of the original model was informally tested against field data [42] yielding encouraging results. As a result of these field data comparisons, it became clear that the original model had to be extended to reflect the fact that the sedimentary features were not always oriented perpendicularly to the prevailing direction of the progressive waves travelling overhead and that the original model was in some sense more difficult to test in the field because, in the vast spans of the ocean, the wave field data showed significant directional information. Parenthetically, the prevalence of the oblique orientation of the bars has also been documented in [5] for the inner shelf. This study presents this extension to the original model to three dimensions. It also clarifies several key issues that were not covered in the original presentation, and it shows how realistic wave spectra can be incorporated in the form of wavepackets [43].

Referring to figure 3, we envision infragravity waves coming into the purview of the model at the line $x = 0$, which is determined in relatively deep water as the location where the waves begin to be significantly influenced by the bottom topography. The x-direction increases as the wave travels shoreward. The spanwise direction, which is the y-coordinate in our reference frame is approximately parallel to the line of constant phase of the incoming waves. The waves propagate shoreward, possibly at an angle with respect to the prevailing direction of maximum gradient of the bottom topography. In the deeper reaches of the shelf, the drift velocity is produced by waves supported by the picnocline, while in the shallower end of the ocean where the water column is more isotropic, the drift velocity is a boundary layer manifestation of the waves on the ocean surface. The extent of the model is limited in the shoreward direction by the disintegration of the interface supporting the internal waves, by the approach to the breaking zone for surface waves, by any singularity in the depth, or by significant energy transfer from low to high frequencies that are ignored by the hydrodynamic modelling. The spanwise direction is limited by the same sorts of issues. Taking advantage of the disparate time-scales for bottom and fluid evolution, we assume that the gently sloping bottom is fixed in the time span in which the water wave begins its trip toward the shore, progresses, and eventually dissipates in the shallow end of

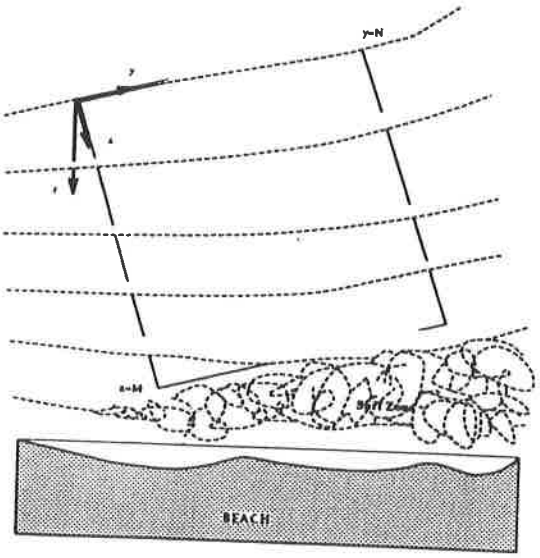

Figure 3. Plan view of the problem.

the model's purview. Taking advantage of this assumption, we then decouple the problem: starting with some initial bottom configuration, we obtain the hydrodynamics of the water surface, which evolves on a time-scale t, say. This in turn yields the drift velocity in the boundary layer; the resultant drift velocity is then used in a transport equation to update the bottom topography, which is evolving on a time scale T that is considerably longer than t.

A few comments should be made about the general mechanism for longshore ripple and sand ridge formation. If a standing-wave pattern exists in the surface waves, whether it be a result of linear or nonlinear effects, the scouring effect of the waves presumably generates ripples obeying a Bragg scattering mechanism (see [29]). This is a first-order phenomenon whose effectiveness in influencing the shape of the bottom topography relies on the existence of both a reflected and an incident wave. Generally, the reflected component becomes weaker and weaker the further it travels seaward. Yet, far from the shore there are abundant fields of large-scale bars. In this deeper region it is suggested that the Bragg mechanism gives way to the second-order, strictly nonlinear theory presented in this study. Thus, we envision that both mechanisms operate along the continental shelf; but in the very near-shore reaches, the first-order theory is prevalent, while in the deeper reaches, the second-order theory prevails.

The second-order drift velocity is not exclusively the result of progressive waves incident on the shore. Reflected waves may also contribute. For very mild slopes and relatively large distances from the shore, however, the reflected component is sometimes quite weak. It is worth emphasizing that the boundary layer drift velocity, which we propose is responsible for sediment movement, is not strictly a result of nonlinear surface waves. However, we believe that both nonlinear and dispersive effects in the water waves influence the features of the sedimentary topography below.

2. Hydrodynamics of the water-wave problem

We believe that striking similarities exists between the typical bar spacing and orientation and the characteristics of the most energetic water long waves. These waves are nonlinear and dispersive. The goal in the present section is to develop a crude but useful model for the important aspects of the overlying hydrodynamics on the surface and in the body of the fluid. This simple model will retain what we think is the bare minimum phenomenology required to test our conjecture both analytically and experimentally. To make the connection clear between the full problem and the crude model, we dedicate this section to the formulation of the simple hydrodynamic model.

Figure 4 is an illustration of the hydrodynamic problem. The free surface is given by $z = \eta(\boldsymbol{r}, t)$ and the bottom by $z = -H(\boldsymbol{r}, T)$, where the notation $\boldsymbol{r} = (x, y)$ is used to denote the transverse coordinates. A thin boundary layer of thickness δ hugs the bottom topography. The spatial domain for the hydrodynamic problem is $\Omega_T = R^2 \times [-H(T) + \delta, \eta(t)] \approx R^2 \times [-H(T), \eta(t)]$, since $\delta \ll |H|$. The T is used to remind us that the scale of time evolution of the bottom is different from that of the fluid environment; hence, it appears here as a parameter. The fluid is subjected solely to gravitational forcing.

The following introduces the notation to be used throughout this study. The velocity field is given by $(\boldsymbol{u}, w)$, where the first entry is the transverse velocity (u, v) and w is the vertical velocity. Position is represented by the vector $(\boldsymbol{r}, z)$. The standard three-component gradient operator is split explicitly into its transverse and vertical coordinates, so that $\nabla_3 \equiv \nabla + \hat{z}\partial_z$. The same convention is followed for the Laplacian operator Δ_3. Incompressibility and irrotationality are assumed to hold in the bulk of the fluid, and its

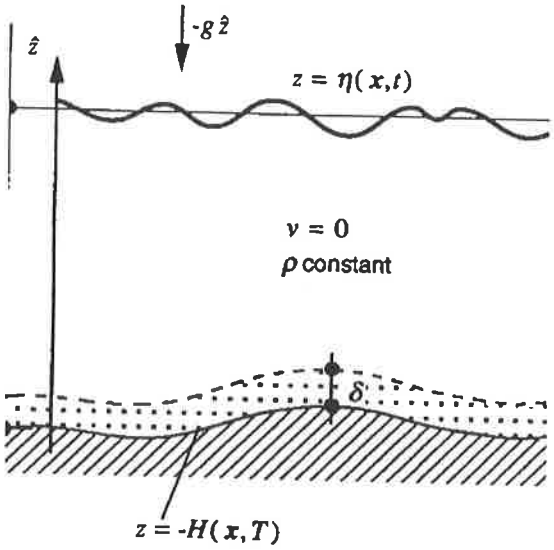

Figure 4. Side view, surface wave problem.

viscosity is assumed negligible in Ω_T. The bottom is taken to be impermeable. This condition, which together with no-slip conditions for the fluid/bottom interface, leads to

$$\phi_z = -\nabla H \cdot \nabla\phi \qquad \text{at } z = -H \tag{1}$$

where

$$(u, w) = \nabla_3\phi\,. \tag{2}$$

Because of the continuity equation, the velocity potential ϕ is harmonic in the flow domain.

At the air–water interface, conservation of momentum requires the pressure to be continuous. The assumed constant value of the pressure immediately above the water is set to zero. Hence, the pressure at the interface when the surface is quiescent is zero. Furthermore, a kinematic condition on the interface leads to $\phi_z = \eta_t + \nabla\phi \cdot \nabla\eta$ at $z = \eta$.

The two-fluid internal wave problem is illustrated in figure 5. The domain is described by $\Omega_1 \approx R^2 \times [-H, \eta]$ and $\Omega_2 = R^2 \times [\eta, D]$. The lower layer (1) has a uniform density ρ_1, and the upper layer (2) a density $\rho_2 < \rho_1$. The velocity field is now given in each layer by $(u, w)_i$, where the subscript refers to layer 1 or 2. The interface between the two fluids is given by $z = \eta(r, t)$ and the bottom by $z = -H(r, T)$. The transverse variable $r = (x, y)$, where x increases shoreward and y is the spanwise coordinate. The fluid is assumed incompressible and irrotational in each layer. In terms of a scalar potential, the velocity is given by $(u, w)_i = \nabla_3\phi_i$. From conservation of mass, the equations of motion within the fluid are $\Delta_3\phi_i = 0$, in Ω_i. At the interface, the pressure is continuous; hence the dynamical boundary condition is $\phi_{i,t} = -\frac{1}{2}|\nabla_3\phi_i|^2 - g\rho_i\eta$, at $z = \eta$.

The bottom, which is assumed impermeable, has a normal velocity that agrees with that of the fluid. Thus $\phi_{1,z} = -\nabla H \cdot \nabla\phi_1$ at $z = -H$. The kinematic condition on the interface is $\frac{D(z-\eta)}{Dt} = 0$, or $\phi_{i,z} = \eta_t + \nabla\phi_i \cdot \nabla\eta$ at $z = \eta$. Finally, we make the simplifying 'rigid-lid' assumption

$$\phi_{2,z} = 0 \qquad \text{at } z = D \tag{3}$$

the constant air–water interface.

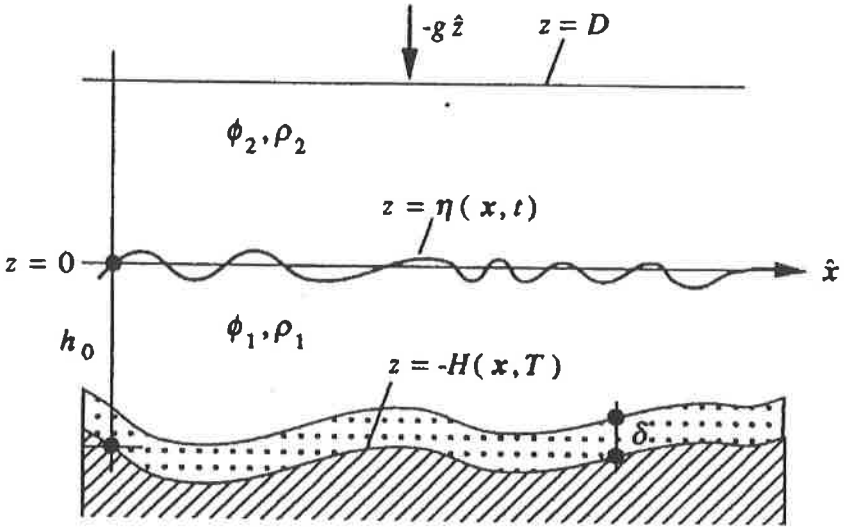

Figure 5. Side view, internal wave problem.

2.1. *Hamiltonian formulation of the hydrodynamic problem*

In this subsection, a useful Hamiltonian formulation of the hydrodynamic problem is presented. This aspect relies heavily on ideas developed by Zakharov and Shabhat [44], Miles [45], Bowman [46], and especially Benjamin [47] and Benjamin and Olver [48].

To begin, we note that the motion of the entire fluid body can be determined once the free surface motion is known. Specifically, if the function η that describes the free surface, and the velocity potential at the free surface, $\Phi \equiv \phi(r, z = \eta, t)$, are known, then Ω_T is determined by η and ϕ is determined by the condition $\phi = \Phi$ at the free surface, together with the boundary condition at the bottom, the fact that ϕ is harmonic in Ω_T, and the asymptotic condition $|\nabla_3 \phi| \to 0$ as $|r| \to \infty$.

Consider the Hamiltonian $E = E(\eta, \Phi)$. The choice of the label E reflects the fact that the Hamiltonian for this problem is conserved and is numerically equal to the sum of the potential energy V and the the kinetic energy K. As shown by Benjamin and Olver [48], the evolution of the free surface is given by the Hamiltonian system

$$\eta_t = \frac{\delta E}{\delta \Phi} \qquad \Phi_t = -\frac{\delta E}{\delta \eta} \tag{4}$$

where E is the Hamiltonian.

We specialize equation (4) for the case of weakly nonlinear shallow-water waves. Define the parameters $\alpha \ll 1$ and $\beta \ll 1$, where α is characteristic of the size of the nonlinearities and β^2 characteristic of the degree of dispersiveness of the surface waves. In terms of physically relevant parameters, $\alpha = a/h_0$ and $\beta = h_0/\lambda$, where a is the typical wave height, h_0 is the characteristic of the fluid column size, and λ is the typical length of the water waves. Further, it is assumed that $O(\alpha) \sim O(\beta^2)$. The Stokes number S, which is a measure of the balance between nonlinear to dispersive effects, is defined as the ratio α/β^2. For $S \ll 1$, nonlinear effects are weak, and only a small portion of energy transfer occurs on moderate space–time scales, so that O(1) nonlinear effects are possible only after very large scales. For $S \sim 1$, inertial effects are of the same order as dispersive effects. In view of this fact, we take $\eta = O(\alpha)$, $\Phi = O(\alpha)$, and the differentiations $\partial_z, \partial_t, \nabla = O(\beta)$. We

note that the Boussinesq system that we are developing is not formally valid for very long evolution distances and is strictly valid for $S = O(1)$, but is quite robust [49]. In this study, the value of S is in the range of 10 to 30, hence the inconsistent appearance of the β^2 term at lowest order. We defer the description of the bottom topography to a later stage, but for now assume that $H = O(1)$, $\nabla H = O(\alpha)$,

An approximation to ϕ, which satisfies the boundary value problem, is

$$\phi(r, z, t) = \Phi(r, t) - \tfrac{1}{2}z^2\nabla^2\Phi(r, t) - z\nabla\cdot(H\nabla\Phi(r, t))$$
$$O(\alpha) \qquad O(\alpha\beta^2) \qquad O(\alpha\beta^2)$$

which can be easily derived by using Rayleigh's trick [50]. The gradient of the above expression

$$U(r, z, t) = u(r, t) - \{z\nabla[\nabla\cdot(Hu(r, t))] + \tfrac{1}{2}z^2\nabla(\nabla\cdot u(r, t))\} \tag{5}$$

gives the velocity anywhere in the inviscid domain of the fluid.

The potential energy is exactly

$$V = \int_{R^2} d^2r\, \tfrac{1}{2}g\eta^2 . \tag{6}$$

The kinetic energy is calculated by using the approximation developed above for the velocity potential, equation (5):

$$K = \int_{R^2} d^2r\left\{\tfrac{1}{2}(H+\eta)(\nabla\Phi)^2 + \tfrac{1}{2}H(\nabla H\cdot\nabla\Phi)^2 - \tfrac{1}{6}H^3(\nabla^2\Phi)^2\right\} \tag{7}$$

which is an expression of $O(\alpha^3\beta^2)$ and $O(\alpha^2\beta^4)$.

Thus, in terms of the velocity at the surface $u \equiv \nabla\Phi$ and the displacement, the energy is $E = V + K_0 + \alpha K_1 + \cdots$, and V is as before. Substituting E in equation (4), to lowest order, yields the wave equation. To the next order,

$$\eta_t + \nabla\cdot\left[(H+\eta)u\right] + \nabla\cdot\left[u\nabla(H^2)\cdot\nabla H + \tfrac{1}{3}\nabla(H^3\nabla\cdot u)\right] = 0 \tag{8}$$

$$u_t + (u\cdot\nabla)u + g\nabla\eta = 0 \tag{9}$$

a version of a Boussinesq system [51]. The Boussinesq system (BSS) is a shallow-water, long-wavelength, weakly nonlinear approximation to the Euler equation which admits bi-directional waves as solutions. The version given by (8) and (9), however, has a couple of troublesome characteristics from the standpoint of modelling a physical situation. Specifically, the system is linearly unstable and rather poor at conveying accurately the full dispersion relation [52]. The instability can be shown by the substitution of plane wave solutions into the linearized version of (8) and (9), and the degree to which the equation's dispersion relation differs appreciably from the full-water wave dispersion is most apparent for the higher wavenumbers. By making changes in the dispersive term (i.e. regularizing), it is possible to overcome the instability problem and improve the agreement between the full dispersion relation and the long-wave limit.

The BSS is regularized by exploiting the specific form of the bottom topography. Using the wave equation obtained for lowest order, and the fact that $\nabla H = O(\alpha)$, we approximate

$$\nabla\cdot\left[u\nabla(H^2)\cdot\nabla H + \tfrac{1}{3}\nabla(H^3\nabla\cdot u)\right] = -\tfrac{1}{3}\nabla\cdot[\nabla(H^2\eta_t)] + O(\alpha) . \tag{10}$$

Thus, the regularized system (RB) adopted in this study, as an approximate model for the water waves, is

$$\eta_t + \nabla\cdot[(H+\eta)u] - \tfrac{1}{3}\nabla\cdot[\nabla(H^2\eta_t)] = 0 \tag{11}$$

$$u_t + (u\cdot\nabla)u + g\nabla\eta = 0 . \tag{12}$$

Since the velocity is in terms of the surface values, rather than in terms of averaged-depth velocity, say, the irrotational condition, with u and v being, respectively, the shoreward and spanwise velocity components, remains in the simple form

$$u_y = v_x \tag{13}$$

which is quite convenient in the development of three-dimensional problems. We could use RB as the working model for the hydrodynamics. However, there are good reasons to simplify the problem further: (i) RB is an initial value problem, requiring that both η and u be known at some time t_0. This is obviously problematic in an ocean setting; (ii) RB (or any of its variants for that matter) is not thoroughly understood from a mathematical standpoint; and (iii) a far simpler description of the water wave problem, which is to be presented below, could still be adequate to test the conjecture.

Using the convention in what follows that new $\leftarrow$ scale $\times$ old, we adopt the scaling

$$t \leftarrow \frac{\sqrt{gh_0}}{\lambda}t \qquad u \leftarrow \frac{\sqrt{h_0}}{\sqrt{g}a}u \qquad \eta \leftarrow \frac{\eta}{a} \qquad h \leftarrow \frac{H}{h_0} \qquad r \leftarrow \frac{r}{\lambda} \tag{14}$$

where h_0 is a characteristic depth of the water column.

In addition, the spanwise dependence is scaled to reflect the fact that waves are propagating primarily in the shoreward direction. To do so, we assume that there is a constant $\xi \ll 1$ such that

$$\mathrm{O}(|\hat{x}\cdot\boldsymbol{K}|) = \xi \times \mathrm{O}(|\hat{y}\cdot\boldsymbol{K}|) \tag{15}$$

for which a consistent uniform expansion of the RB exists and that is physically relevant. If nonlinear, dispersive, and weak y variation effects are to balance, the size of the constant must be of the order of $\alpha^{1/2}$. Proceeding,

$$y \leftarrow \xi y \qquad \hat{y}\cdot\boldsymbol{u} \leftarrow \xi\hat{y}\cdot\boldsymbol{u} \tag{16}$$

which will alter the regularized system but will not affect the irrotational condition, equation (13). This scaling is known as the 'parabolic approximation' [53].

For the internal wave problem, with conjugate variables η and $\boldsymbol{U} \equiv \rho_2\nabla\phi_2 - \rho_1\nabla\phi_1$ the Hamiltonian system that yields the description of the dynamics of the internal waves takes the form

$$\eta_t = -\nabla\cdot\left(\frac{\delta E}{\delta \boldsymbol{U}}\right) \qquad \boldsymbol{U}_t = -\nabla\left(\frac{\delta E}{\delta\eta}\right) \tag{17}$$

where the Hamiltonian E is numerically equal to the sum of the potential and the kinetic energy for this problem.

The potential energy is simply

$$V = \int_{R^2} \mathrm{d}^2r\, \tfrac{1}{2}g(\rho_1 - \rho_2)\eta^2\,. \tag{18}$$

The total kinetic energy is the sum of contributions from both layers; thus

$$K = \rho_1\int_{R^2}\mathrm{d}^2r\int_{-H}^{\eta}\tfrac{1}{2}\,|\nabla_3\phi_1|^2\,\mathrm{d}z + \rho_2\int_{R^2}\mathrm{d}^2r\int_{-\eta}^{D}\tfrac{1}{2}\,|\nabla_3\phi_2|^2\,\mathrm{d}z = K_1 + K_2\,. \tag{19}$$

Define the parameters $\alpha \ll 1$, and $\beta \ll 1$. Assume that $\mathrm{O}(\alpha) \sim \mathrm{O}(\beta^2)$, and take $H = \mathrm{O}(1)$, $\nabla H = \mathrm{O}(\alpha)$, $\eta = \mathrm{O}(\alpha)$, $\Phi = \mathrm{O}(\alpha)$. Further, consider the differentiations ∂_z, ∂_t, $\nabla = \mathrm{O}(\beta)$.

Referring to equation (7), we calculate the kinetic energy in the lower layer using an approximation for the velocity potential,

$$\phi_1(r,z,t) = \Phi_1(r,t) - \tfrac{1}{2}z^2\nabla^2\Phi_1(r,t) - z\nabla\cdot(H\nabla\Phi_1(r,t))$$
$$\qquad\quad O(\alpha) \qquad O(\alpha\beta^2) \qquad\qquad O(\alpha\beta^2)$$

so that

$$K_1 = \rho_1 \int_{R^2} d^2r\left\{\tfrac{1}{2}(H+\eta)(\nabla\Phi_1)^2 + \tfrac{1}{2}H(\nabla H\cdot\nabla\Phi_1)^2 - \tfrac{1}{6}H^3\left(\nabla^2\Phi_1\right)^2\right\} \tag{20}$$

which is an expression of $O(\alpha^3\beta^2)$ and $O(\alpha^2\beta^4)$.

The boundary condition given by (3) can be exploited to find K_2 as a surface integral. Using Green's theorem and assuming that the gradients of the potential tend to zero as $|r| \to \infty$, we have

$$K_2 = -\rho_2 \int_{R^2} d^2r\, \nabla\Phi_1\nabla\Phi_2\,. \tag{21}$$

Define the pseudo-differential operator $G \equiv -k\coth(HkD)$. Its precise structure is a result of satisfying the boundary conditions on the interface and on the ocean surface. Adding the expressions for K_1 and K_2, using the definition of $\boldsymbol{U}$, and the operator G, we obtain as the total kinetic energy

$$K = \tfrac{1}{2}\int_{R^2} d^2r\left\{\frac{1}{\rho_1}(H+\eta)U^2 + \frac{H^2\rho_2}{\rho_1^2}\boldsymbol{U}\cdot G\boldsymbol{U} + \frac{\rho_2 H}{\rho_1^2}(\nabla H\cdot\boldsymbol{U})^2\right\} + O(\alpha^3\beta^2) \tag{22}$$

or rearranging

$$K = \tfrac{1}{2}\int_{R^2} d^2r\left\{\frac{1}{\rho_1}\left[(H+\eta) - \frac{H^2\rho_2}{\rho_1^2 D}\right]U^2 + \frac{H^2\rho_2}{\rho_1^2}\boldsymbol{U}\cdot M\boldsymbol{U} + \frac{\rho_2 H}{\rho_1^2}(\nabla H\cdot\boldsymbol{U})^2\right\} + O(\alpha^3\beta^2) \tag{23}$$

where $M = \frac{I}{D} + G = \frac{1}{D} - k\coth(HkD)$.

Depending on the size of D/λ, there are three physically distinct possibilities:

- If $D/\lambda \ll 1$, then $\boldsymbol{U}\cdot M\boldsymbol{U} = O(\alpha^2 D/\lambda^2)$, and $M \approx 1/D - \frac{1}{3}D\nabla^2$. For this case, the terms $\eta\boldsymbol{U}\cdot\boldsymbol{U}$ and $\boldsymbol{U}\cdot M\boldsymbol{U}$ balance if $\alpha^2 D/\lambda^2 \sim 1$. A Boussinesq system is obtained.
- If $D/\lambda \sim 1$, then $\boldsymbol{U}\cdot M\boldsymbol{U} = O(\alpha^2/\lambda)$. For this case, if $\alpha\lambda^2/D \sim 1$, the result is the intermediate long-wave equation.
- If $D/\lambda \gg 1$, then $\boldsymbol{U}\cdot M\boldsymbol{U} = O(\alpha^2/\lambda)$, and $M \approx |k|$. If $\alpha\lambda \sim 1$, the outcome is the Benjamin–Ono equation.

Note that this last case corresponds to a very deep upper layer, lying over a thinner lower layer, and hence is not considered relevant in this study. In the ocean setting the density stratification is most appropriately described by a continuous function with respect to depth. However, if a two-fluid approximation is adequate, the case relevant to the problem at hand among those presented above is the first one.

By substituting the expressions for the potential and kinetic energy, equations (18) and (23), into (17), the general equation for the dynamics of the internal wave field is obtained:

$$\begin{aligned}\eta_t &= -\nabla\cdot\left\{\left[\frac{1}{\rho_1}(H+\eta) - \frac{H^2\rho_2}{\rho_1^2 D}\right]\boldsymbol{U}\right\} - \frac{\rho_2}{\rho_1^2}\nabla\cdot\left\{H(\nabla H)^2\boldsymbol{U} + H^2 M\boldsymbol{U}\right\}\\ \boldsymbol{U}_t &= -\nabla\cdot\left\{\frac{1}{2\rho_1^2}\boldsymbol{U}\cdot\boldsymbol{U} + (\rho_1-\rho_2)g\eta\right\}.\end{aligned} \tag{24}$$

The result from linear theory may be recovered by neglecting second- and higher-order terms in (24). The solutions proportional to $\exp\{i(kx - \omega t)\}$ satisfy

$$\begin{aligned} \omega\eta &= \left(\frac{1}{\rho_1} - \frac{\rho_2 H}{\rho_1^2 D} + \frac{\rho_2 HM}{\rho_1^2}\right) kHU \\ \omega U &= k(\rho_1 - \rho_2) g\eta\,. \end{aligned} \tag{25}$$

Thus,

$$c^2 \equiv \frac{\omega^2}{k^2} = \frac{g(\rho_1 - \rho_2)}{\rho_1}\left[1 - \frac{\rho_2}{\rho_1} Hk \coth(kD)\right]. \tag{26}$$

The relevant case in this study is the first one:

$$\begin{aligned} \eta_t &= -\nabla\cdot\left\{\frac{1}{\rho_1}(H+\eta)\boldsymbol{U}\right\} - \frac{\rho_2}{\rho_1^2}\nabla\cdot\left\{H(\nabla H)^2\boldsymbol{U} + \tfrac{1}{3}H^2 D\nabla\nabla\cdot\boldsymbol{U}\right\} \\ \boldsymbol{U}_t &= -\nabla\cdot\left\{\frac{1}{2\rho_1^2}\boldsymbol{U}\cdot\boldsymbol{U} + (\rho_1 - \rho_2)g\eta\right\}. \end{aligned} \tag{27}$$

Equation (24) is linearly unstable [55]. To circumvent this problem, we carry out the *ad hoc* procedure that 'regularizes' the equation. The lowest-order relations

$$\eta_t = -\nabla\cdot\left\{\frac{1}{\rho_1}H\boldsymbol{U}\right\} \qquad \boldsymbol{U}_t = -\nabla\{(\rho_1 - \rho_2)g\eta\} \tag{28}$$

are used to modify the troublesome parts of the dispersive terms to obtain the regularized model for the hydrodynamics relevant in this study, namely,

$$\begin{aligned} \eta_t &= -\nabla\cdot\left\{\frac{1}{\rho_1}(H+\eta)\boldsymbol{U}\right\} + \frac{D\rho_2}{3\rho_1^2}\nabla\cdot[\nabla(H\eta_t)] \\ \boldsymbol{U}_t &= -\nabla\left\{\frac{1}{2\rho_1^2}\boldsymbol{U}\cdot\boldsymbol{U} + (\rho_1 - \rho_2)g\eta\right\}. \end{aligned} \tag{29}$$

Let $\gamma \equiv \frac{(\rho_1-\rho_2)}{\rho_1}$ be the Boussinesq parameter, and let the typical thickness of the lower layer be h_0. The scaling adopted here is

$$\begin{aligned} t &\leftarrow \frac{\sqrt{gh_0}\,t}{\lambda} \qquad \boldsymbol{U} \leftarrow \frac{\sqrt{h_0}\,\boldsymbol{U}}{\rho_1\sqrt{g}a} \qquad \eta \leftarrow \frac{\eta}{a} \\ h &\leftarrow \frac{H}{h_0} \qquad d \leftarrow \frac{D}{h_0} \qquad \boldsymbol{r} \leftarrow \frac{\boldsymbol{r}}{\lambda} \end{aligned} \tag{30}$$

where the convention new $\leftarrow$ scale $\times$ old is being used. Equation (29) is, in scaled variables,

$$\begin{aligned} &\eta_t + \nabla\cdot\left\{\frac{1}{\rho_1}(h + \alpha\eta)\boldsymbol{U}\right\} - \mathrm{d}\beta^2\frac{\rho_2}{3\rho_1}\nabla\cdot[\nabla(h\eta_t)] = 0 \\ &\boldsymbol{U}_t + \nabla\left\{\tfrac{1}{2}\boldsymbol{U}\cdot\boldsymbol{U} + \gamma\eta\right\} = 0\,. \end{aligned} \tag{31}$$

Additionally, the spanwise variables are scaled to reflect the weak spanwise dependence of the waves.

2.2. Description of the bottom topography and the wavepacket description of the water waves

Laboratory data [29] suggests that there are several time-scales in this problem: a fast time-scale t, and slower time-scale $\tau = O(\alpha t)$, which measure the evolution of the fluid quantities. There is yet another slow time-scale $T = O(\alpha' t)$, where $\alpha' = O(\alpha)$ and is assumed to be fixed by the minimal time-scale $T > t$ in which appreciable changes occur in the forcing of the infragravity waves at $x = 0$. This slow time-scale is characteristic of the evolution of the bottom topography. For the sake of simplicity and clarity of presentation, we shall set $\alpha' = \alpha$ here. Some brief comments on this important issue of time-scales will be made in the last section of this paper.

In addition, the data suggests that the typical height and slopes of the longshore sand ridges are such that $\varepsilon = O(\nabla^n h) = O(\alpha)$. Such a restriction is consistent with the approximations made in the RB. Furthermore, the type of longshore sand ridge under consideration is such that the measure of longshore spatial variation is larger than the spatial variations of the fluid quantities. It is suggested that the sand ridge shoreward variation be $X = \alpha x$. Hence, two scales of shoreward variation exist, so that

$$\partial_x \to \partial_x + \alpha \partial_X \tag{32}$$

$$\partial_t \to \partial_t + \alpha \partial_\tau . \tag{33}$$

Thus, in scaled variables the bottom, is

$$h(X, y, T) = 1 + \varepsilon f(X, y, T) \tag{34}$$

where the function $f = O(1)$.

Let us consider the surface wave problem in detail. By substituting an expansion of the form

$$\begin{aligned} \eta &= f_0 + \alpha^1 f_1 + \alpha^2 f_2 + \cdots \\ u &= g_0 + \alpha^1 g_1 + \alpha^2 g_2 + \cdots \end{aligned} \tag{35}$$

into equations (11)–(13), and matching order by order, it is possible to solve for the surface quantities to lowest orders in α. Our interest here is limited to the lowest-order theory. We refer the interested reader to [56] for the details of the higher-order theory.

At the first two orders we obtain the relations, with $G(X, y, T) = \frac{\varepsilon f(X, y, T)}{\alpha}$,

$$\begin{aligned} &\alpha^0\text{: } \mathcal{L}\eta_0 = 0 \\ &\alpha^1\text{: } \mathcal{L}\eta_1 = \mathcal{G}_1(\eta_0, u_0, v_0, G; x, X, y, t) \end{aligned} \tag{36}$$

where

$$\mathcal{L} = \partial_{tt} - \partial_{xx} - \tfrac{1}{3}\beta^2 \partial_{xxtt} \tag{37}$$

and $\mathcal{L}$ is a linear operator that shows up at every order. The inhomogeneous term $\mathcal{G}_1$ is

$$\begin{aligned} \mathcal{G}_1 = {} & (1 + \beta^2 \partial_{tt}/3)\eta_{0yy} + G(1 + 2\beta^2 \partial_{tt}/3)\eta_{0xx} + 2(1 + \beta^2 \partial_{tt}/3)\eta_{0xX} \\ & + (u_0^2/2)_x - (u_0 \eta_0)_{xt} - (1 - 2\beta^2 \partial_{xx}/3)\eta_{0\tau} . \end{aligned} \tag{38}$$

We assume that the shoreward velocity is

$$\begin{aligned} u(x, X, y, t) = {} & \sum_{j=1}^{2} [a_j(X, y) + O(\alpha)] e^{i(k_j x - \omega_j t)} + \text{CC} \\ & + \sum_{j=1}^{2} [b_j(X, y) + O(\alpha)] e^{i(-k_j x - \omega_j t)} + \text{CC} \end{aligned} \tag{39}$$

where CC stands for the complex conjugate of the expression immediately preceding its appearance. The a's and b's are the complex incident and reflected wavepackets, respectively. These wavepackets are centred at k_j and have support $\Delta k_j < k_j$. The reality of the physical variables implies that $a_{-j} = a_j^*$ and $b_{-j} = b_j^*$. The spanwise velocity at the surface must then be

$$v(x, X, y, t) = \sum_{j=1}^{2} -\frac{\mathrm{i}}{k_j}[a_{jy}(X, y) + \mathrm{O}(\alpha)]\mathrm{e}^{\mathrm{i}(k_j x - \omega_j t)} + \mathrm{CC}$$
$$+ \sum_{j=1}^{2} -\frac{\mathrm{i}}{k_j}[b_j(X, y) + \mathrm{O}(\alpha)]\mathrm{e}^{\mathrm{i}(-k_j x - \omega_j t)} + \mathrm{CC} \tag{40}$$

in order to satisfy (13). Since, to lowest order, $u_{0t} + \eta_{0x} = 0$, an expression for the surface amplitude is readily available: the replacement of the lowest-order velocity into the momentum equation yields

$$\eta_0 = \sum_{j=1}^{2} \frac{\omega_j}{k_j}[a_j(X, y) + \mathrm{O}(\alpha)]\mathrm{e}^{\mathrm{i}(k_j x - \omega_j t)} + \mathrm{CC}$$
$$+ \sum_{j=1}^{2} \frac{\omega_j}{k_j}[b_j(X, y) + \mathrm{O}(\alpha)]\mathrm{e}^{\mathrm{i}(-k_j x - \omega_j t)} + \mathrm{CC}\,. \tag{41}$$

The appropriateness of making use of a small number of packets comes from field data. Figure 6 suggests that most of the energy in the waves is found in the first few packets [57]. The figure also shows the shifting of energy from lower frequencies to higher ones as the wave travels shoreward over a decreasing water column depth.

The ansatz in (39) implies that $\eta_{0\tau} = 0$ is satisfied. The conditions required for the omission of such a term as well as its implications are the subject of a concurrent study [58]. This form of the solution is extremely convenient because it turns the initial value problem into a boundary value problem.

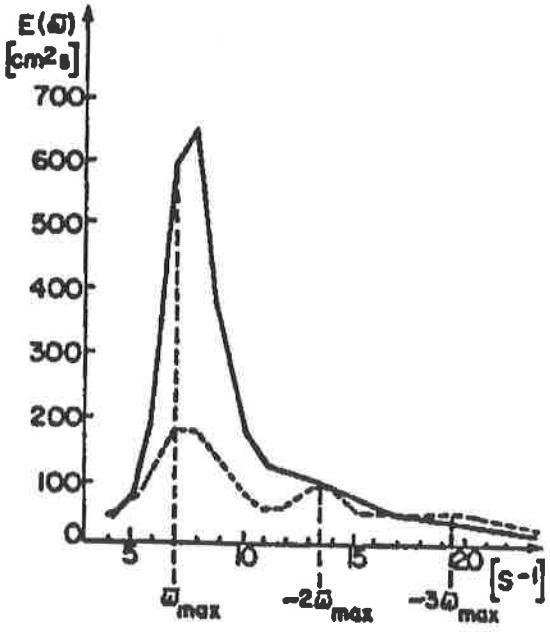

Figure 6. Energy for shallow water waves in the Southern Baltic Sea: (——)$h_0 = 6.0m$, – – –$h_0 = 2.0m$. From Druet *et al* [57].

A solution of the form given by (39)–(41) is valid provided that the following relation holds between the frequency and the wavenumber:

$$\omega_j^2 - \frac{k_j^2}{1 + \frac{1}{3}\beta^2 k_j^2} = 0 \tag{42}$$

which gives the dispersion relation for the jth carrier, the positive root k_j corresponding to the shoreward-directed wave, and the negative to the seaward wave.

The solution must also satisfy a compatibility condition. Since the dispersion relation for gravity water waves is such that $\omega'(\kappa) > 0$ and $\omega''(\kappa) < 0$, perfect resonance is not possible. At most we expect what we refer to as 'slight resonance.' With $k_2 = 2k_1 - \delta$, $\omega_2 = 2\omega_1$, where the detuning parameter $\delta \leqslant 0$, the compatibility condition is

$$\frac{jk_1}{2\pi}\int_{X_0}^{X_0+2\pi/jk_1} \mathrm{e}^{\pm \mathrm{i}jk_1 x}(\mathcal{G}_j + \mathcal{G}_j^*)\,\mathrm{d}x = 0 \qquad \text{where} \quad j = 1, 2 \tag{43}$$

starred quantities are conjugated.

Application of the compatibility condition to the lowest-order terms in (38) yields, after some algebra, the evolution equations for the packet centres in (39) and (41):

$$\begin{aligned}
&a_{1x} + \mathrm{i}\varepsilon f D_1 E_1 a_1 - \mathrm{i}\xi F_1 a_{1yy} + \mathrm{i}\alpha D_1 S_1 \mathrm{e}^{-\mathrm{i}\delta x} a_1^* a_2 = 0\\
&a_{2x} + \mathrm{i}\varepsilon f D_2 E_2 a_2 - \mathrm{i}\xi F_2 a_{2yy} + \mathrm{i}\alpha D_2 S_2 \mathrm{e}^{+\mathrm{i}\delta x} a_1^2 = 0\\
&b_{1x} - \mathrm{i}\varepsilon f D_1 E_1 b_1 + \mathrm{i}\xi F_1 b_{1yy} - \mathrm{i}\alpha D_1 S_1 \mathrm{e}^{+\mathrm{i}\delta x} b_1^* b_2 = 0\\
&b_{2x} - \mathrm{i}\varepsilon f D_2 E_2 b_2 + \mathrm{i}\xi F_2 b_{2yy} - \mathrm{i}\alpha D_2 S_2 \mathrm{e}^{-\mathrm{i}\delta x} b_1^2 = 0
\end{aligned} \tag{44}$$

having substituted back $X = ax$. The constants are

$$\begin{aligned}
&D_j = \left[2\left(1 - \tfrac{1}{3}\beta^2\omega_j^2\right)\right]^{-1} \qquad E_j = k_j\left(1 - \tfrac{2}{3}\beta^2\omega_j^2\right) \qquad F_j = \frac{1}{2k_j}\\
&S_1 = \frac{k_2 - k_1}{\omega_1}\left\{k_2 - k_1 + \omega_1\left(\frac{\omega_1}{k_1} + \frac{\omega_2}{k_2}\right)\right\} \qquad S_2 = 2\frac{\left(k_1^2 + 2\omega_1^2\right)}{\omega_2}.
\end{aligned} \tag{45}$$

Equation (44), along with appropriate boundary conditions, determines in an approximate way the ocean surface. The incident and reflected waves are decoupled owing to the assumptions and restrictions on the spatial variation of the bottom topography. If the spatial scales of variation in the bottom topography in the shoreward direction are of the same order as those of the surface waves, then scattering plays an important role in the energetics of these surface waves; hence the reflected component must be included even if the backwash is negligible. If, on the other hand, the longshore sand ridges being considered were

$$h(x, X, y, T) = 1 + \varepsilon f(x, X, y, T) \tag{46}$$

the resulting surface equations, to lowest order, would be

$$\begin{aligned}
&a_{1x} - \mathrm{i}\varepsilon f D_1 E_1 \gamma_1 a_1 + \mathrm{i}\varepsilon f D_1 E_1 \mu_1^- b_1 - \mathrm{i}\xi F_1 a_{1yy} + \mathrm{i}\alpha D_1 S_1 \mathrm{e}^{-\mathrm{i}\delta x} a_1^* a_2 = 0\\
&a_{2x} - \mathrm{i}\varepsilon f D_2 E_2 \gamma_2 a_2 + \mathrm{i}\varepsilon f D_2 E_2 \mu_2^- b_2 \mathrm{e}^{2\mathrm{i}\delta x} - \mathrm{i}\xi F_2 a_{2yy} + \mathrm{i}\alpha D_2 S_2 \mathrm{e}^{+\mathrm{i}\delta x} a_1^2 = 0\\
&b_{1x} + \mathrm{i}\varepsilon f D_1 E_1 \gamma_1 b_1 - \mathrm{i}\varepsilon f D_1 E_1 \mu_1^+ a_1 + \mathrm{i}\xi F_1 b_{1yy} - \mathrm{i}\alpha D_1 S_1 \mathrm{e}^{+\mathrm{i}\delta x} b_1^* b_2 = 0\\
&b_{2x} + \mathrm{i}\varepsilon f D_2 E_2 b_2 - \mathrm{i}\varepsilon f D_2 E_2 \mathrm{e}^{-\mathrm{i}2\delta x} \mu_2^+ a_2 + \mathrm{i}\xi F_2 b_{2yy} - \mathrm{i}\alpha D_2 S_2 \mathrm{e}^{-\mathrm{i}\delta x} b_1^2 = 0
\end{aligned} \tag{47}$$

to $O(\delta/X)$, with

$$\gamma_j = \frac{jk_1}{2\pi}\int_0^{2\pi/jk_1}(f_{xx} + 2ik_j f_x - k_j^2 f)\,dx$$
$$\mu_j^- = \frac{jk_1}{2\pi}\int_0^{2\pi/jk_1}(f_{xx} + 2ik_j f_x - k_j^2 f)e^{-2ijk_1x}\,dx \tag{48}$$
$$\mu_j^+ = \frac{jk_1}{2\pi}\int_0^{2\pi/jk_1}(f_{xx} + 2ik_j f_x - k_j^2 f)e^{+2ijk_1x}\,dx\,.$$

The most striking differences between the way (44) and (47) describe the surface are that, in the latter case, the terms involving the bottom topography, which attenuate and modulate the waves as they propagate, involve the bottom topography, its slope, and its curvature; and the energy in the reflected wave does not depend exclusively on the boundary conditions.

The same procedure applied to the internal wave problem yields the same system of equations as in (44) and (47), but the constants are defined as

$$D_j = 1/2\left(1 - d\frac{\rho_2\beta^2\omega_j^2}{3\rho_1}\right) \qquad E_j = k_j\left(\gamma - d\frac{2\rho_2\beta^2\omega_j^2}{3\rho_1}\right) \qquad F_j = \frac{1}{2k_j}$$
$$S_1 = \frac{k_2 - k_1}{\omega_1}\left\{k_2 - k_1 + \frac{\omega_1}{\gamma}\left(\frac{\omega_1}{k_1} + \frac{\omega_2}{k_2}\right)\right\} \qquad S_2 = \frac{2}{\omega_2}k_1^2 + 2\omega_1^2\,. \tag{49}$$

The dispersion relation for the internal wavepackets is

$$\omega_j^2 - \frac{k_j^2}{\gamma + d\beta^2\frac{\rho_2 k_j^2}{3\rho_1}} = 0\,. \tag{50}$$

For three-wavepacket weak resonance, the relation among the frequency and wavenumbers $\omega_j = j\omega_1$, $k_2 = 2k_1 - \delta$, and $k_3 = 3k_1 - \Delta$ is given by the dispersion relation. The procedure is the same as for the two-wave group case and yields

$$a_{1x} + i\varepsilon f D_1 E_1 a_1 - i\xi F_1 a_{1yy} + i\alpha D_1 S_{211} e^{-i\delta x} a_1^* a_2 + i\alpha D_1 S_{321} e^{i\Delta x} a_2^* a_3 = 0$$
$$a_{2x} + i\varepsilon f D_2 E_2 a_2 - i\xi F_2 a_{2yy} + i\alpha D_2 S_2 e^{+i\delta x} a_1^2 + i\alpha D_2 S_{312} e^{i\Delta x} a_1^* a_3 = 0 \tag{51}$$
$$a_{3x} + i\varepsilon f D_3 E_3 a_3 - i\xi F_3 a_{3yy} + i\alpha D_3 S_3 e^{-i\Delta x} a_1 a_2 = 0$$

to $O(\delta/X)$. The constants are, with subscripts 1, 2 or 3,

$$D_j = 1/2\left(1 - \frac{d\rho_2\beta^2\omega_j^2}{3\rho_1}\right) \qquad E_j = k_j\left(\gamma - \frac{2d\rho_2\beta^2\omega_j^2}{3\rho_1}\right)$$
$$F_j = \frac{1}{2k_j} \qquad S_3 = \frac{k_2 + k_1}{\omega_3}\left\{k_2 + k_1 + \frac{3\omega_1}{\gamma}\left(\frac{\omega_1}{k_1} + \frac{\omega_2}{k_2}\right)\right\} \tag{52}$$
$$S_2 = \frac{2}{\omega_2}k_1^2 + 2\omega_1^2 \qquad S_{ijl} = \frac{k_i - k_l}{l\omega_1}\left\{k_i - k_j + \frac{l\omega_1}{\gamma}\left(\frac{\omega_i}{k_i} + \frac{\omega_j}{k_j}\right)\right\}.$$

We will concentrate on the two-wavepacket case in this study.

3. The mass transport problem

The drift velocity is the second-order steady-state flow that is created by the passage of overlying water waves in the sediment-laden boundary layer that hugs the bottom topography. The boundary layer is assumed to have a characteristic thickness $\delta_{bl} \ll h_0$. The sediment in the boundary layer is assumed, without loss of generality, to move from place

to place at a rate equal to the drift velocity. To compute the drift velocity, we must find the fluid velocity immediately outside of the sediment-laden boundary layer. This can be determined for both the internal and surficial wave case simultaneously: in what follows, $\gamma = \frac{\rho_1 - \rho_2}{\rho_1}$ for the internal wave problem and $\gamma = 1$ for the surface wave case. From equation (5) in scaled variables, the shoreward velocity is explicitly

$$\begin{aligned} U_b &\equiv \gamma \hat{x} \cdot \boldsymbol{U}(\boldsymbol{r}, -h, t) \\ &= \gamma u(\boldsymbol{r}, t) - \gamma\beta^2\{-h[(hu_{xx}(\boldsymbol{r}, t)) + \xi(hv_{xy}(\boldsymbol{r}, t))] + \tfrac{1}{2}h^2(u_{xx}(\boldsymbol{r}, t) + \xi v_{xy}(\boldsymbol{r}, t))\} \end{aligned} \tag{53}$$

and the spanwise velocity

$$\begin{aligned} V_b &\equiv \gamma \hat{y} \cdot \boldsymbol{U}(\boldsymbol{r}, -h, t) \\ &= \gamma v(\boldsymbol{r}, t) - \gamma\beta^2\{-h[(hu_{xy}(\boldsymbol{r}, t)) + \xi(hv_{yy}(\boldsymbol{r}, t))] + \tfrac{1}{2}h^2(u_{xy}(\boldsymbol{r}, t) + \xi v_{yy}(\boldsymbol{r}, t))\} \end{aligned} \tag{54}$$

in the neighbourhood of the boundary layer. If we neglect the reflected component, the bottom velocities are, to lowest order

$$\begin{aligned} U_{0b} &= \gamma u_0 + \tfrac{1}{2}\gamma\beta^2 h^2 u_{0xx} \\ &= \sum_{j=1}^{2} C_j a_j(X, y) e^{i(k_j x - \omega_j t)} + \text{CC} \\ V_{0b} &= \gamma v_0 + \tfrac{1}{2}\gamma\beta^2 (h^2)_y u_{0x} + \tfrac{1}{2}\gamma\beta^2 h^2 u_{0xy} \\ &= -\mathrm{i}\sum_{j=1}^{2} \frac{1}{k_j}\left[C_j a_{jy}(X, y) + \tfrac{1}{2}\mathrm{i}\gamma\beta^2 k_j (h^2)_y\right] e^{\mathrm{i}(k_j x - \omega_j t)} + \text{CC} \end{aligned} \tag{55}$$

where $C_j = \gamma(1 - \frac{1}{2}\beta^2 k_j^2 h^2)$.

3.1. Hydrodynamics of the boundary layer

In the boundary layer the transverse momentum, vertical momentum, and the continuity equations are, respectively,

$$\begin{aligned} &\boldsymbol{u}_t + \boldsymbol{u} \cdot \nabla \boldsymbol{u} + \bar{w}\boldsymbol{u}_z = -\frac{1}{\rho}\nabla p + \nu\Delta \boldsymbol{u} + \nu \boldsymbol{u}_{zz} \\ &\bar{w}_t + \boldsymbol{u} \cdot \nabla \bar{w} + \bar{w}\bar{w}_z = -\frac{1}{\rho} p_z + g + \nu\Delta\bar{w} + \nu\bar{w}_{zz} \\ &\nabla \cdot \boldsymbol{u} + \bar{w}_z = 0 \end{aligned} \tag{56}$$

where ν is the assumed isotropic eddy viscosity. Across the boundary layer the flow velocity changes from zero at the bottom boundary to some finite value characteristic of the exterior inviscid fluid. The derivatives with respect to z of any flow quantity are thus, in general, much greater than those with respect to x or y. Hence, within the boundary layer, $|\nabla \boldsymbol{u}| \ll |\boldsymbol{u}_z|$, $|\nabla^2 \boldsymbol{u}| \ll |\boldsymbol{u}_{zz}|$, etc. We conclude that the transverse momentum in (56) is well approximated by

$$\boldsymbol{u}_t + \boldsymbol{u} \cdot \nabla \boldsymbol{u} + \bar{w}\boldsymbol{u}_z = -\frac{1}{\rho}\nabla p + \nu \boldsymbol{u}_{zz}\,. \tag{57}$$

The velocity $\bar{w}$ must also be small. The continuity statement in (56) suggests that the boundary layer and $\bar{w}$ are of equal order of smallness. Therefore, none of the terms on the left-hand side of (57) can be neglected. If $\sqrt{gh_0}$ is representative of the magnitude of the velocity $\boldsymbol{u}$ and λ represents a distance in the transverse direction over which $\boldsymbol{u}$ changes

appreciably, then $(\sqrt{gh_0})^2/\lambda = O(\boldsymbol{u}\cdot\nabla\boldsymbol{u})$. Since δ_{bl} is the boundary layer thickness, $\nu\sqrt{gh_0}/\delta_{bl}^2$ is a measure of νu_{zz}. Thus,

$$O(\delta_{bl}^2 R/\lambda^2) = 1 \qquad \text{where} R = \frac{\sqrt{gh_0}\lambda}{\nu}. \tag{58}$$

The dimensionless constant R is the Reynolds number. We assume that the boundary layer does not change significantly as a function of wave frequency. Thus, λ can be replaced by h_0 in R, so that $R = \sqrt{gh_0}h_0/\nu$. We arrive, then, at a working definition for the boundary layer thickness:

$$\delta_{bl} = \sqrt{\nu/h_0(gh_0)^{1/2}} \tag{59}$$

which is non-dimensionalized by dividing by h_0. In this scaling, it is implied that the size of the Reynolds number and the boundary layer thickness are controlled mostly by the viscous effects (i.e. the size of ν).

To estimate the size of $\tilde{w}$, we conclude from the continuity condition in (56) that

$$\tilde{w} = O(\beta\sqrt{gh_0}R^{-1/2}). \tag{60}$$

With equation (60) in hand, we can infer from the vertical momentum balance that $p_z = O(\delta_{bl})$; that is, the pressure is approximately constant throughout the layer.

For high Reynolds number flow, with $\delta_{bl}n = z + h$, where $\bar{z} = R^{1/2}z$ and $w = R^{1/2}\bar{w}$, the equations for the boundary layer are

$$\begin{aligned} &\beta u_t + \alpha\beta[uu_x + \alpha v u_y] + \alpha w u_n = -\frac{\beta}{\alpha}p_x + u_{nn} \\ &\beta v_t + \alpha\beta[uv_x + \alpha v v_y] + \alpha w v_n = -\frac{\beta}{\alpha}p_y + v_{nn} \\ &p_n = O(\delta_{bl}) \qquad \beta(u_x + \alpha v_y) + w_n = 0 \end{aligned} \tag{61}$$

having invoked the scaling that reflects weak y dependence of the flow as well. A locally flat bed has been assumed. In contrast, suppose that the bed had some finite curvature K, say. This would change the vertical momentum balance in (61) to

$$p_n = KO(u^2) \tag{62}$$

but the pressure change across the layer is still of $O(\delta_{bl})$, so we are justified in the assumption that the bed is locally flat.

The following boundary data is used to solve (61):

$$u = v = w = 0 \qquad \text{at} \quad n = 0 \tag{63}$$

and

$$u \to U_b \qquad v \to V_b \qquad n \to \infty. \tag{64}$$

The velocity (U_b, V_b) immediately outside of the layer gives rise to the following pressure gradients:

$$\begin{aligned} -\frac{\beta}{\alpha}p_x &= \beta U_{bt} + \alpha\beta(U_b U_{bx} + \alpha V_b U_{by}) \\ -\frac{\beta}{\alpha}p_y &= \beta V_{bt} + \alpha\beta(U_b V_{bx} + \alpha V_b V_{by}). \end{aligned} \tag{65}$$

We thus have all the required information to solve for the velocities in the boundary layer. Performing the usual expansion

$$\begin{aligned} u &= \tilde{u}_0 + \alpha\tilde{u}_1 \cdots \\ v &= \tilde{v}_0 + \alpha\tilde{v}_1 \cdots \end{aligned} \tag{66}$$

we obtain as the lowest-order equations

$$\begin{aligned} &\beta\tilde{u}_{0t} - \tilde{u}_{0nn} = \beta U_{0bt} \qquad \beta\tilde{v}_{0t} - \tilde{v}_{0nn} = \beta V_{0bt} \\ &p_{0n} = 0 \qquad \beta\tilde{u}_{0x} + \tilde{w}_{0n} = 0\,. \end{aligned} \tag{67}$$

A solution of (67) of the form

$$\tilde{u}_l = \sum_{j=1}^{2} \alpha^l P_l(x, y, n) e^{i(k_j x - \omega_j t)} + \text{cc} \tag{68}$$

subject to the boundary conditions given by (63) and (64), is found by integrating (67). The same procedure is used to obtain $\tilde{v}$. The result is

$$\begin{aligned} \tilde{u}_0 &= \sum_{j=1}^{2} C_j a_j \left(1 - e^{-n\Lambda_j}\right) e^{i(k_j x - \omega_j t)} + \text{CC} \\ \tilde{v}_0 &= i \sum_{j=1}^{2} k_j \left(\beta^2 \left(h^2\right)_y a_j/2 - C_j a_{jy}/k_j^2\right)\left(1 - e^{-n\Lambda_j}\right) e^{i(k_j x - \omega_j t)} + \text{CC} \\ \tilde{w}_0 &= i\beta \sum_{j=1}^{2} k_j C_j a_j \left(1 - n\Lambda_j - e^{-n\Lambda_j}\right)/\Lambda_j e^{i(k_j x - \omega_j t)} + \text{CC} \end{aligned} \tag{69}$$

where $\Lambda_j = (1 - i)\sqrt{\beta\omega_j/2}$. The vertical velocity $\tilde{w}$ is found by integrating the continuity equation.

With the expressions for the velocity in the boundary layer, we proceed to obtain the drift velocity, the source of net movement of the suspended sedimentary particles. The drift velocity is the time average displacement rate of a fluid particle. Define the time average of the quantity A as

$$\langle A \rangle \equiv \frac{\omega}{2\pi} \int_t^{t+2\pi/\omega} A(s)\,ds = \frac{1}{\tau} \int_t^{t+\tau} A(s)\,ds\,. \tag{70}$$

The drift velocity [22], is obtained to lowest order by substituting the expressions in (70) in

$$\begin{aligned} \mathcal{U} &= \langle u_1 \rangle + \left\langle \int^t u_0\, d\tilde{t}\, u_{0x} \right\rangle + \left\langle \int^t w_0\, d\tilde{t}\, u_{0n} \right\rangle \\ \mathcal{V} &= \langle v_1 \rangle + \left\langle \int^t u_0\, d\tilde{t}\, v_{0x} \right\rangle + \left\langle \int^t w_0\, d\tilde{t}\, v_{0n} \right\rangle. \end{aligned} \tag{71}$$

3.2. The mass transport equation

Since the mean slopes in the regions of principal interest here are very low, down-slope gravitational transport, which is important in the coastal environment, plays a negligible role in the formation of sand ridges. We assume that sediment movement in regions sufficiently removed from the shoaling region is accomplished primarily by suspension. Hence, we adopt results from the Longuett-Higgins theory to characterize the effect of the water waves on the fluid motion in the boundary layer. Furthermore, since the ratio of bar height to separation is significantly below the critical value of 0.1 (which has been identified by Sleath [13] as the value over which flow in the boundary layer separates behind the crests of the bars and vortex formation takes place), the flow in the boundary layer is adequately characterized by the lowest-order dynamical quantities. In what follows, the fluid wave field is assumed to be entirely represented by the incident wave. Further, we assume that

the viscous boundary layer is sediment-laden, composed of cohesionless, rarely interacting sand particles.

The sediment concentration ρ in coastal environments has a very weak influence on the fluid flow [59]. Typical values for the concentration are $\rho \sim 10^{-3}$–10^{-4} ppm, and this situation is assumed thoughout the shelf. Chapalain [59] and Boczar-Karakiewicz *et al* [60] concluded that time-independent and vertically uniform parameters of eddy viscosity and eddy diffusivity provide satisfactory accuracy for sediment morphology models on the shelf. In this study we adopt a very simple model for the sediment concentration [13].

An equation of continuity for the sediment concentration is the advection–diffusion equation

$$\rho_t + \nabla \cdot (\boldsymbol{u}\rho) + [(w - v_f)\rho]_n = 0 \tag{72}$$

where v_f is the sediment 'fall velocity' and $n = (z+h(X, y, T))/\delta_{bl}$. For simplicity assume that, apart from random fluctuations, $\boldsymbol{u}$ and ρ do not vary much over small transverse spatial scales, so that the second term of the above equation may be neglected. In light of this, the sediment concentration changes at a rate $\partial\rho/\partial n$ proportional to the vertical flux. Hence,

$$w\rho = -\gamma\rho_n \tag{73}$$

where γ is the diffusivity constant.

The flux, which is the product of the concentration and the velocity, can be split into a time-dependent part C^t and a time-independent part C^m. Boczar-Karakiewicz *et al* [7] found that in the sand ridge areas, the ratio $C^t/C^m = \mathrm{O}(10^{-2})$ for the off-shore case. This situation is assumed to apply throughout the shelf, so that the sediment concentration is represented solely by its time-independent part. Employing this assumption and substituting (73) into (72), we have as the equation for sediment concentration

$$\gamma\rho_n + v_f\rho = 0\,. \tag{74}$$

The boundary condition may be taken as

$$\frac{\gamma}{v_f}\frac{\partial\rho}{\partial n} = P(\boldsymbol{r}) \tag{75}$$

where $P(\boldsymbol{r})$ has the flavour of Svendsen's [61] empirical 'pick-up function', which incorporates such effects as the degree of wave asymmetry and skewness of sediment flux, and a Shield's parameter, which sets a threshold fluid velocity at which sediment will be picked up, based on the sediment particles' buoyancy and geometry and on the fluid's velocity field and viscocity.

Solving equation (74), we obtain as the sediment concentration

$$\rho = P(\boldsymbol{r})\mathrm{e}^{-\sigma n} \tag{76}$$

where $\sigma = v_f/\gamma$. The fall velocity v_f is species-dependent. It is either measured or estimated by calculating the balance of drag to buoyant forces for a particle falling freely into a static fluid. The diffusivity constant γ is hard to estimate: sedimentologists usually measure its value in the field.

For the sake of clarity, the mass transport equation is derived by assuming transverse dependence in the x direction only. The generalization to variations in y follow in a straightforward manner. Let $T \in [0, \infty)$ and $\Pi_T \in \mathcal{R}^1 \times [h(T), \zeta]$, where $\zeta \geqslant h(T)+\delta_{bl}$, be the boundary layer time–space domain, and consider a differential 'volume' element in such a domain, as shown in figure 7, which is bounded on the bottom by the ocean topography and on the top by a flat lid $z' = \zeta$. It is assumed that the sediment concentration ρ is entirely negligible for $z' > \zeta$ and moves on fast time-scales. In what follows ρ: $\Pi_T \longmapsto \mathcal{R}^1$.

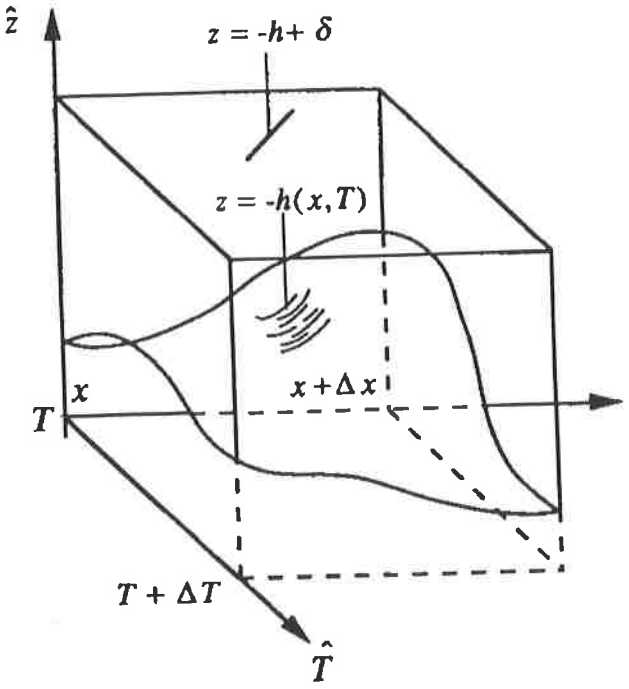

Figure 7. Volume element used in the derivation of the mass trasport equation.

The sediment concentration and drift velocity are thought to be $C^1(\Pi_T)$, and the bottom topography $h \in C^1(T)$, and piecewise linear in Π_T.

The mass flux per unit length at x in a time interval $[T, T + \Delta T]$ is given by

$$\int_T^{T+\Delta T} d\tau \int_{h(x,\tau)}^{\zeta} dz'\, \rho(x,z')\mathcal{U}(x,z') \equiv \int_T^{T+\Delta T} d\tau \int_{h(x,\tau)}^{\zeta} dz'\, M(x,z')\,. \tag{77}$$

Consider a portion of the region, say $[x, x + \Delta x]$, in a time interval $[T, T + \Delta T]$. Since mass cannot spontaneously vanish or be created, the net amount of sediment between point x and $x + \Delta x$ must be compensated for by a change in the concentration of the sediment or by a topographical change in the bottom surface. The flux difference in the space and time intervals $[x, x + \Delta x]$, $[T, T + \Delta T]$ is thus

$$\int_T^{T+\Delta T} d\tau \int_{h(x+\Delta x,\tau)}^{\zeta} dz'\, M(x+\Delta x, z') - \int_T^{T+\Delta T} d\tau \int_{h(x,\tau)}^{\zeta} dz'\, M(x,z') \tag{78}$$

and the total mass in the given portion at time T is given by

$$\int_x^{x+\Delta x} d\xi \int_{h(\xi,T)}^{\zeta} dz'\rho(\xi,z')\,. \tag{79}$$

The change in total mass in a time interval $[T, T + \Delta T]$ resulting from net accumulation is given by

$$\int_x^{x+\Delta x} d\xi \int_{h(\xi,T+\Delta T)}^{\zeta} dz\, \rho(\xi,z') - \int_x^{x+\Delta x} d\xi \int_{h(\xi,T)}^{\zeta} dz'\, \rho(\xi,z') \tag{80}$$

or equivalently,

$$\int_x^{x+\Delta x} d\xi \int_{h(\xi,T)}^{h(\xi,T+\Delta T)} dz'\, \rho(\xi,z')\,. \tag{81}$$

Equating (78) and (81), dividing by $\Delta x \Delta T$, and formally taking the limit as Δx and ΔT go to zero, we obtain, on the right-hand side,

$$\begin{aligned}
&\lim_{\Delta T\to 0\Delta x\to 0} \frac{1}{\Delta x \Delta T} \int_x^{x+\Delta x} \mathrm{d}\xi \int_{h(\xi.T)}^{h(\xi.T+\Delta T)} \mathrm{d}z'\, \rho(\xi, z') \\
&\qquad \sim \lim_{\Delta T\to 0\Delta x\to 0} \frac{1}{\Delta x \Delta T} \int_x^{x+\Delta x} \mathrm{d}\xi \int_{h(\xi.T)}^{h(\xi.T)+\Delta T \frac{\partial h(\xi.T)}{\partial T}} \mathrm{d}z'\, \rho(\xi, z') \\
&\qquad = \rho(x, h(x,T)) \frac{\partial h(x,T)}{\partial T} \qquad (82)
\end{aligned}$$

and on the other side of the equation,

$$\begin{aligned}
&\lim_{\Delta T\to 0\Delta x\to 0} \frac{1}{\Delta x \Delta T} \int_T^{T+\Delta T} \mathrm{d}\tau \left\{ \int_{h(x+\Delta x.\tau)}^{\zeta} \mathrm{d}z'\, M(x+\Delta x, z') - \int_{h(x.\tau)}^{\zeta} \mathrm{d}z'\, M(x,z') \right\} \\
&\qquad = \lim_{\Delta T\to 0\Delta x\to 0} \frac{1}{\Delta x \Delta T} \\
&\qquad \int_T^{T+\Delta T} \left\{ \int_{h(x+\Delta x.\tau)}^{\zeta} \mathrm{d}z' \left[M(x,z') + \Delta x \frac{\partial M}{\partial x}(x,z') + \cdots \right] - \int_{h(x.\tau)}^{\zeta} M(x,z') \right\} \\
&\qquad = \lim_{\Delta T\to 0\Delta x\to 0} \frac{1}{\Delta x \Delta T} \Delta x \int_{h(x.\tau)+\Delta x \frac{\partial h}{\partial x}}^{\zeta} \mathrm{d}z' \frac{\partial M}{\partial x}(x,z') \\
&\qquad = \int_{h(x.T)}^{\zeta} \mathrm{d}z' \frac{\partial M}{\partial x}(x,z') . \qquad (83)
\end{aligned}$$

Hence, the mass transport equation is

$$\frac{\partial h(x,T)}{\partial T} = \frac{K'}{\rho(x,h(x,T))} \frac{\partial}{\partial x} \int_{h(x.T)}^{\zeta} \rho(x,z') \mathcal{U}(x,z')\, \mathrm{d}z' \qquad (84)$$

where K' is a constant of proportionality. Since the boundary layer is assumed to be very thin, we may define the mass transport flux as

$$\mu \equiv \int_0^{\delta_{bl}} \rho(x,z') \mathcal{U}(x,z')\, \mathrm{d}z' \qquad \nu \equiv \int_0^{\delta_{bl}} \rho(x,z') \mathcal{V}(x,z')\, \mathrm{d}z' \qquad (85)$$

so that the transport equation now reads

$$\frac{\partial h(x,T)}{\partial T} = \frac{K}{\rho_0} \mu_x . \qquad (86)$$

The generalization of (86) to one more space dimension is

$$\frac{\partial h(x,y,T)}{\partial T} = \frac{K}{\rho_0} (\mu_x + \nu_y) \qquad (87)$$

where μ and ν are the shoreward mass flux and the longshore mass flux, respectively. Note that when weak y dependence scaling is adopted in (87), the longshore mass flux is $O(\alpha)$ smaller than all other quantities in the equation.

In the remainder of this paper, we assume, for simplicity, that the sediment concentration is constant and equal to ρ_0 in the boundary layer. In terms of (71), and upon use of (85), the calculation of the mass flux components, to lowest order, is

$$\mu = \sum_{j=1}^{2} \frac{2k_j C_j^2 |a_j|^2}{\omega_j \sigma_j} \mathcal{I}_{1j} + \sum_{j=1}^{2} \frac{\beta k_j C_j^2 |a_j|^2}{\sigma_j^3} \mathcal{I}_{2j} + \mathrm{CC} \qquad (88)$$

where

$$\mathcal{I}_{1j} = \sigma_j\delta_{bl} - \tfrac{1}{2}\beta\sigma_j - \tfrac{3}{2} + \tfrac{1}{2}(1 - \beta\sigma_j)\mathrm{e}^{-2\sigma_j\delta_{bl}} + \mathrm{e}^{-\sigma_j\delta_{bl}}[\cos\sigma_j\delta_{bl} - \sin\sigma_j\delta_{bl}][1 - \beta\sigma_j(\sigma_j\delta_{bl} + 1)] \tag{89}$$

and

$$\mathcal{I}_{2j} = \tfrac{3}{2}(\tfrac{1}{2} - \sigma_j\delta_{bl}) + \mathrm{e}^{-2\sigma_j\delta_{bl}}/4 - \mathrm{e}^{-\sigma_j\delta_{bl}}[1 + \delta_{bl}\sigma_j]\cos\sigma_j\delta_{bl} + 2\mathrm{e}^{-\sigma_j\delta_{bl}}\sin\sigma_j \tag{90}$$

for the shoreward mass flux, and

$$\nu = \sum_{j=1}^{2} \frac{\mathrm{i}C_j^2 a_j^* a_{jy}}{\omega_j\sigma_j}\mathcal{J}_j + \mathrm{O}(\beta^3) + \mathrm{cc} \tag{91}$$

for the longshore directed mass flux, with

$$\mathcal{J}_j = \sigma_j\delta_{bl} - 1 - \tfrac{1}{2}\left(1 - \mathrm{e}^{-2\sigma_j\delta_{bl}}\right) + \mathrm{e}^{-\sigma_j\delta_{bl}}(\cos\sigma_j\delta_{bl} - \sin\sigma_j\delta_{bl}) + \beta\Lambda_j\left[\tfrac{1}{2}\left(1 + \mathrm{e}^{-2\sigma_j\delta_{bl}}\right) + \mathrm{e}^{-\Lambda_j\delta_{bl}}(\mathrm{i}\delta_{bl}\sigma_j/2 - 1)\right]. \tag{92}$$

The quantities $\mathcal{I}_{11}$, $\mathcal{I}_{21}$, and $\mathcal{J}_1$ are plotted parametrically in figures 8–10.

Before proceeding, two important remarks are in order. First, we note that the bottom need not be slightly perturbed to initiate the development of bars. Second, the time-scale discrepancy may be estimated by examining the ratio of the magnitude of the time rate of change of the bottom to the Eulerian velocity. Such a comparison leads in a straightforward manner to the conclusion that $t/T = \mathrm{O}(\alpha)\mathrm{O}(\delta_{bl})\mathrm{O}(\rho) \sim \mathrm{O}(10^{-7})$, assuming that the boundary layer thickness is typically $\mathrm{O}(10^{-2}h_0)$ and the sediment concentration is $\mathrm{O}(10^{-4})$ ppm.

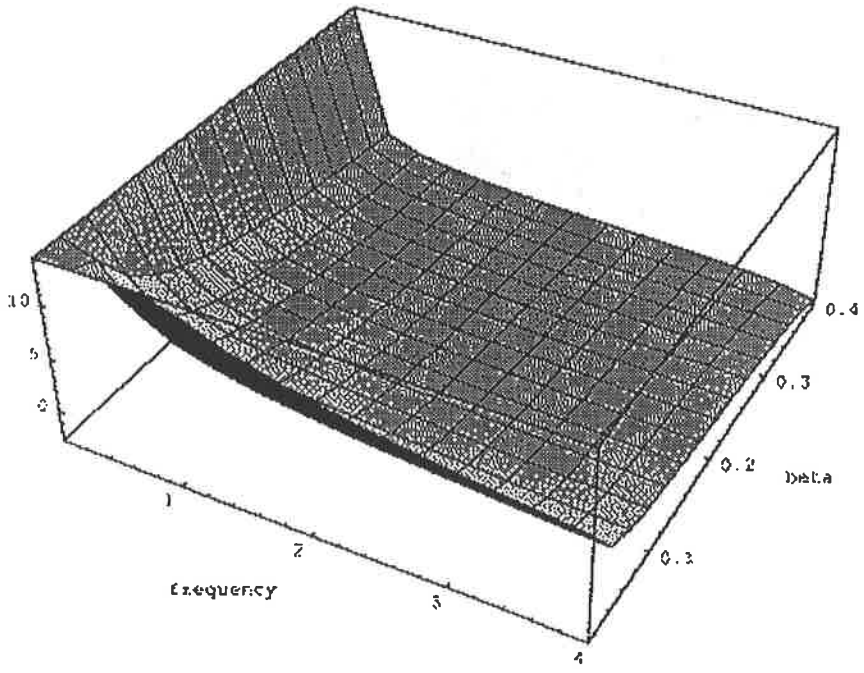

Figure 8. Variation of $\mathcal{I}_{11}$, with $\delta_{bl} = 1.0$ fixed.

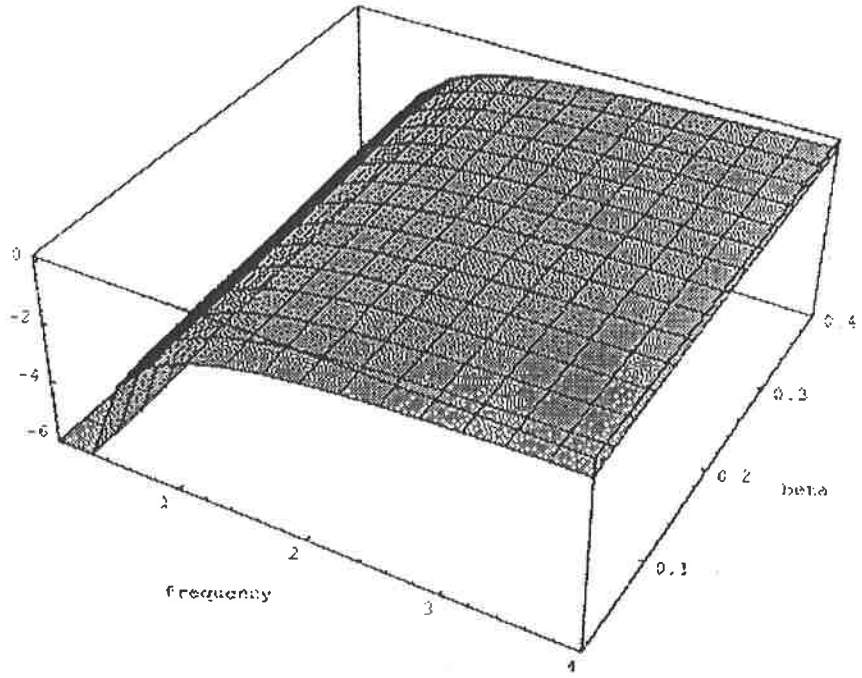

Figure 9. Variation of $\mathcal{I}_{21}$, with $\delta_{bl} = 1.0$ fixed.

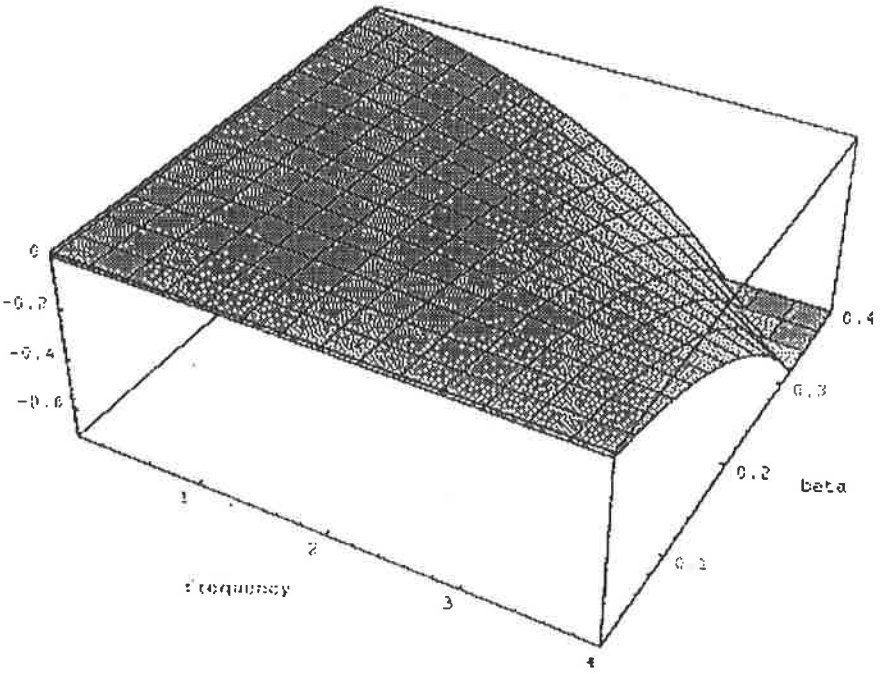

Figure 10. Parametric plot of $\mathcal{J}_1$, with $\delta_{bl} = 1.0$ fixed.

4. Qualitative features of the solutions to the full model

Some of the qualitative features of the full model are presented in this section, with examples computed numerically with the fixed-point method, which is described in [62]. The main points of the section are (i) to present the effects of different initial bottom configurations and boundary conditions on the surface and on the eventual bottom topography after the passage of many surface waves, and (ii) to show that the smaller reflected wave plays a relatively minor role in determining the shape of the ocean surface and therefore of the sand ridge topography when the bottom is assumed to be very mildly sloped.

To better discern the effects of different bottom topographies on the waves and on the eventual bottom topography after the passage of many waves, we now turn to the case in which the initial bottom configurations are strictly x-dependent and the boundary conditions are constant. Briefly, in this case, a larger number of bars form when the gradient is slight, the distance separating the bars increases seaward for the positively sloped case, and initial bottom discontinuities in the x-direction tend to get 'smoothed out' after the passage of many waves.

Figure 11 shows the bottom topography, which was

$$f(x, y, 0) = \begin{cases} 0.005x & x > 180.0 \\ 0 & \text{otherwise} \end{cases} \tag{93}$$

at $T = 0$. The lighter curve represents the bottom profile at $T = 20\Delta T$; the heavier curve is the bottom at $T = 80\Delta T$. The parameters are $\alpha = 0.1$, $\varepsilon = 0.2$, $\beta = 0.36$ and $\omega_1 = 1.2$. For the same range of parameters, figure 12 shows the effect on the surface and on the eventual bottom of an initial topography that is approximately tuned to the interaction length of the surface waves.

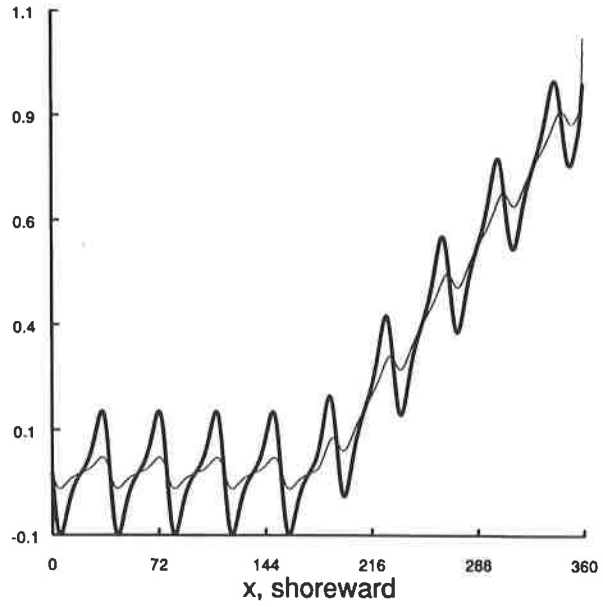

Figure 11. Cross section of $f(x, y, T)$. The bottom was initially sloped but featureless. The heavier curve represents the bottom at $T = 80\Delta T$, whereas the lighter curve represents the bottom at $T = 20\Delta T$.

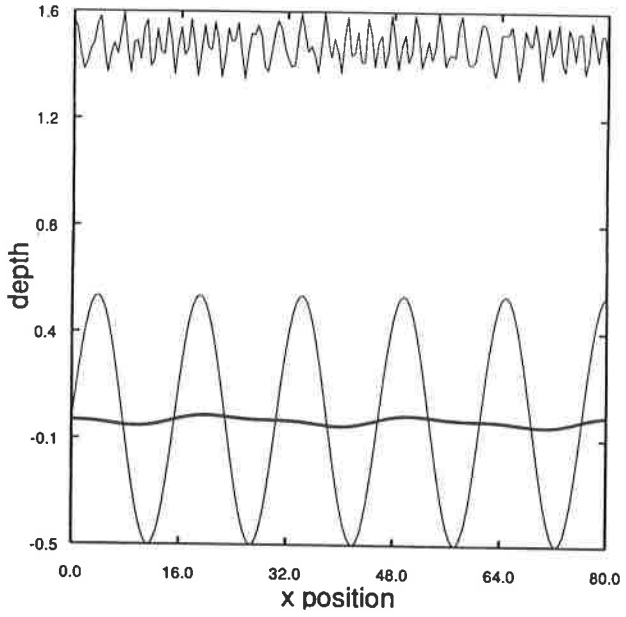

Figure 12. Effect of a tuned bottom, $f = 0.5\sin(0.412x)$ at $T = 0$, on the eventual topography and ocean surface: light full curve. Bottom at $T = 100\Delta T$: heavy full curve.

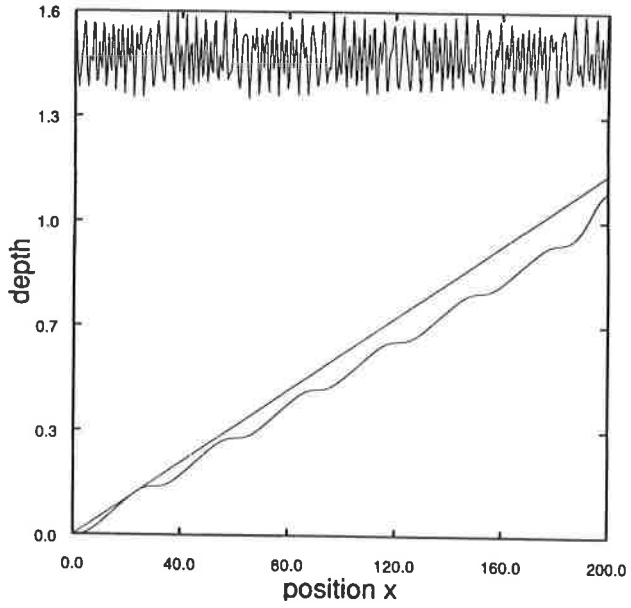

Figure 13. Ocean surface at $T = 0$. Bottom at $T = 400$, for $f(x, y, T = 0) = 0.006x$. $a_1(x = 0) = 0.5$, $a_2(x = 0) = 0.01$.

Waves at $T = 0$ that are travelling normal to the shore over topography initially described by $f = 0.006x$ are displayed in figure 13. Superimposed, but not drawn to scale, is the eventual bottom topography. Figure 14 shows the evolution of an initially

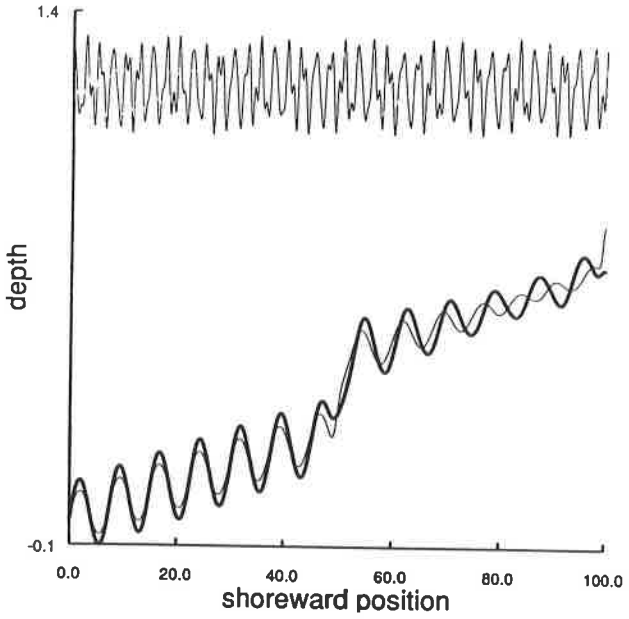

Figure 14. The fate of the topography which initially contained a step, shown at three different times.

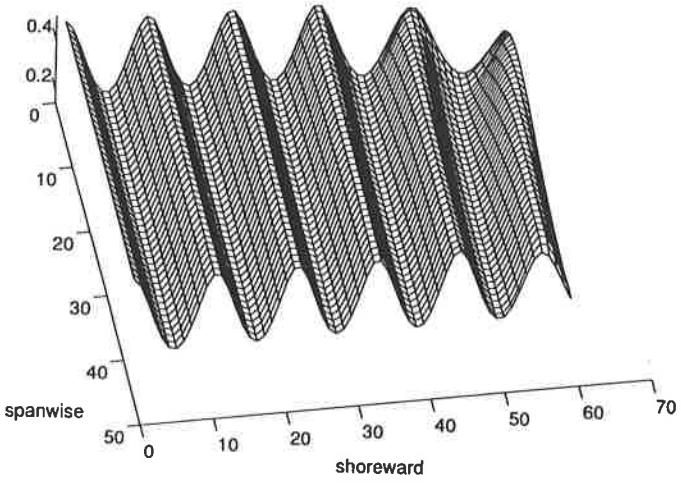

Figure 15. Refraction of a_1 due to the bottom topography: $f(x, y) = -0.005y$ shown at $T = 0$.

stepped bottom at three different times. For these figures $\alpha = 0.1$, $\varepsilon = 0.2$, $\beta = 0.08$, and $\omega_1 = 1.8$.

A bottom, which initially had gradients in the y direction, bends the water waves, affecting the eventual bottom topography by producing a series of bars with refractive features. Consider, for example, the case in which the initial bottom topography is $f(x, y) = -0.005y$, with all other parameters as before, except $\omega_1 = 1.2$. Figure 15 shows a_1 at $T = 0$. A striking way in which refraction takes place can be seen in the case for which the boundary conditions at $x = 0$ are y-dependent. The case for which $f(x, y) = 0$ at $T = 0$ and the boundary conditions are $\mathcal{A}_1 = 0.5 + 0.001y$ and $\mathcal{A}_2 = 0.02 + 0.001y$, corresponding to an incoming gravity wave that has slightly higher amplitude at one end than at the other,

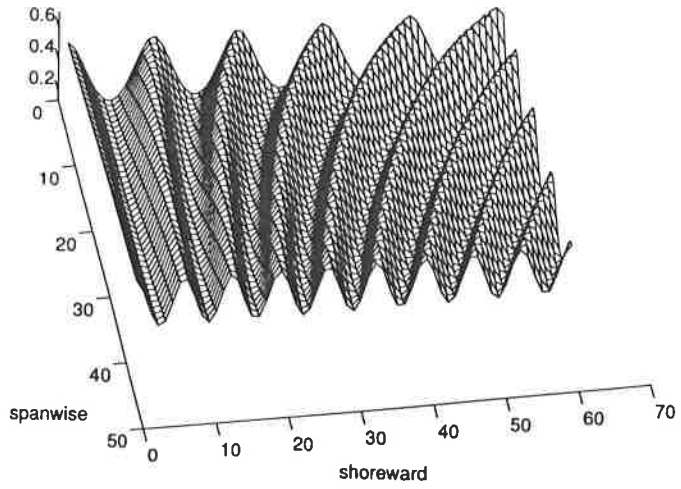

Figure 16. Refraction due to boundary conditions. a_1 at $T = 0$.

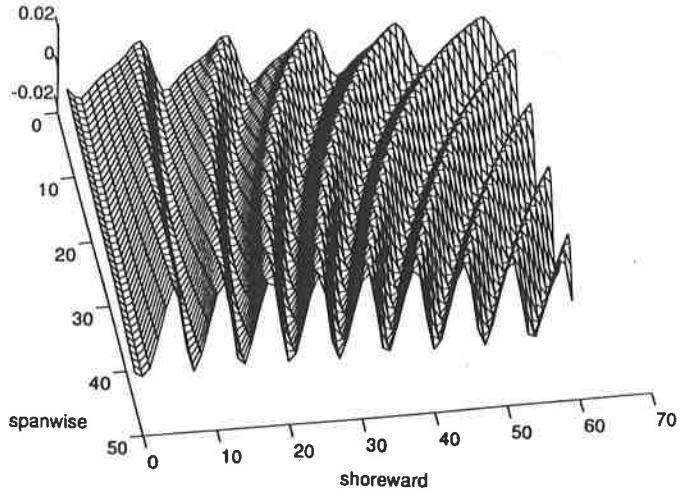

Figure 17. Refraction due to boundary conditions. Bottom at $T = 100\Delta T$.

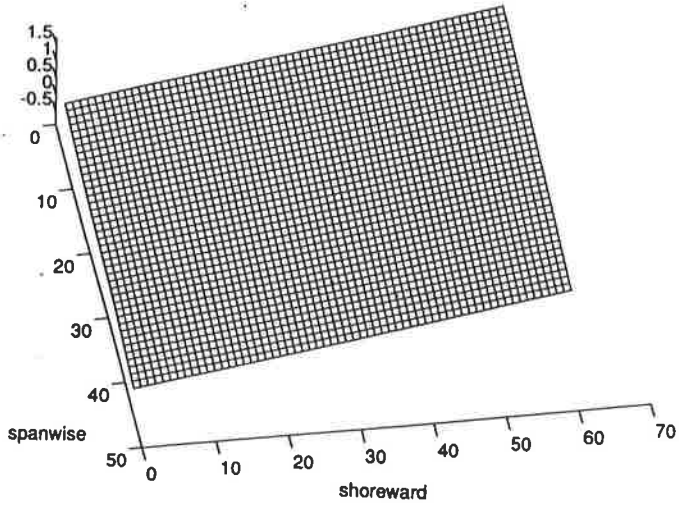

Figure 18. Evolution of bottom topography. $T = 0$.

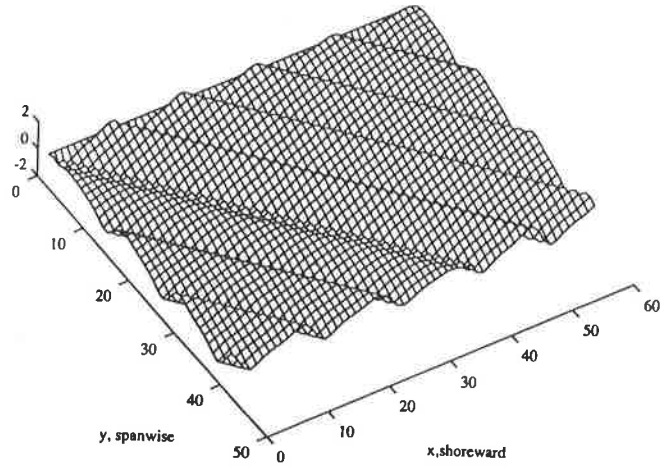

Figure 19. Evolution of bottom topography at $T = 40\Delta T$. Shown here is the difference between the new bottom and the original topography.

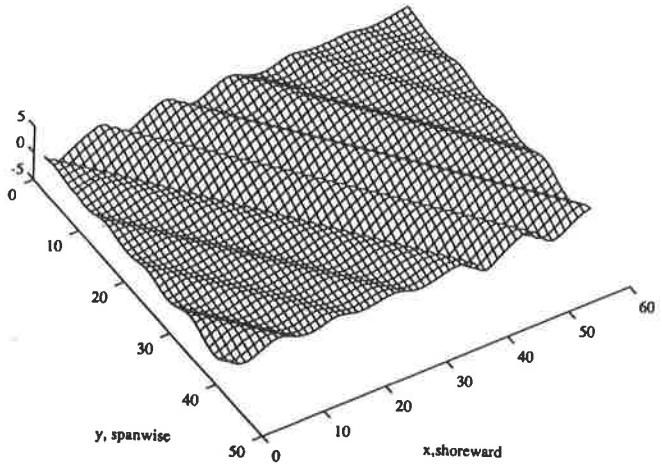

Figure 20. Evolution of bottom topography. $T = 100\Delta T$. Shown here is the difference between the new bottom and the original topography.

is shown in figures 16 and 17 for $a_1(T = 0)$ and $f(T = 100\Delta T)$, respectively. The eventual fate of a bottom that was initially smooth but sloped, $f(x, y) = 0.0075x - 0.005y$, is illustrated in figures 18–20. Compare these with figure 15. The boundary conditions are $\mathcal{A}_1 = 0.5$ and $\mathcal{A}_2 = 0.02$.

Shown in figure 21 is the cross section of $a_1(x)$ and $b_1(x)$, and in figure 22 a comparison of the eventual bottom with and without contributions from the reflected field. Both figures were computed by using (44), with $\mathcal{A}_1 = 0.5$, $\mathcal{A}_2 = 0.01$, $\mathcal{B}_1 = 0.2$ and $\mathcal{B}_2 = 0$; $\varepsilon = 0.2$, $\alpha = 0.1$, $\beta = 0.08$. The bottom was $f(x, y) = 0.006x$ at $T = 0$. The domain was 200 units long.

As was discussed in section 2, the reflected and incident fields are completely decoupled, owing to the assumptions made concerning the bottom topography. The deformations on the bottom topography due to the reflected component are entirely determined by the amount of energy in the boundary conditions. Hence, it is necessary to include the reflected component when the seagoing wave backwash is not negligible.

Interesting configurations are achieved when the above-mentioned effects are combined. Figure 23 illustrates the refraction pattern on one of the packet centres for which $\mathcal{A}_1 = 0.5 - 0.001y$, $\mathcal{A}_2 = 0.1 - 0.001y$, and the bottom at $T = 0$ was $f(x, y) = 0.01y$.

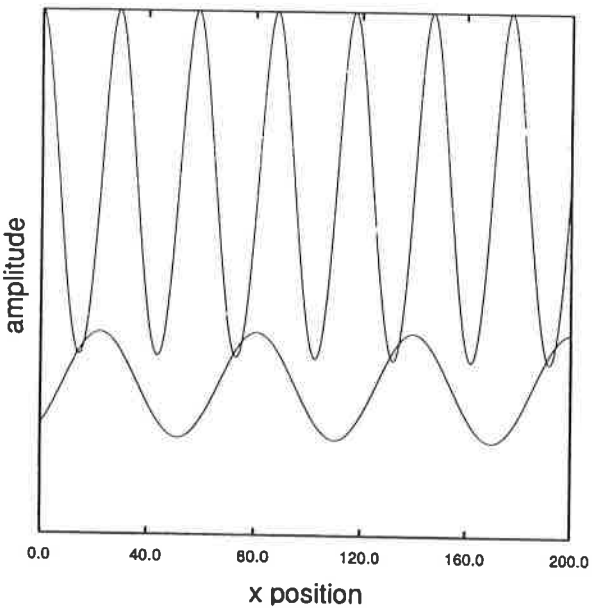

Figure 21. Profile of a_1 and b_1, for $f(x, y) = 0.006x$. $\mathcal{A}_1 = 0.5$, $\mathcal{B}_1 = 0.2$.

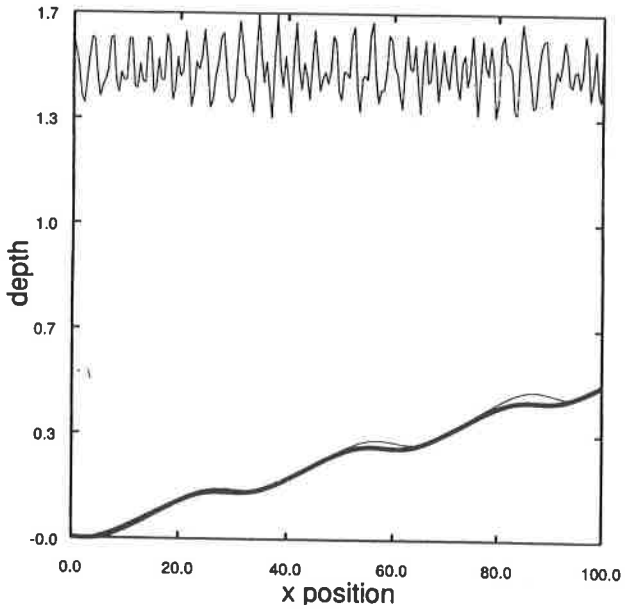

Figure 22. Effect of a bi-directional surface wave field on the eventual bottom configuration. Initially, $f(x, y, 0) = 0.006x$. The heavy full curve is the bottom resulting from a strictly shoreward-directed wave.

Another curious change in pattern direction is illustrated in figure 24. In this case $\mathcal{A}_1 = 0.5 - 0.001y$, $\mathcal{A}_2 = 0.1 + 0.001y$, and the bottom at $T = 0$ is $f(x, y) = 0.01y$. All the parameters in figure 24 are the same as those in figure 23.

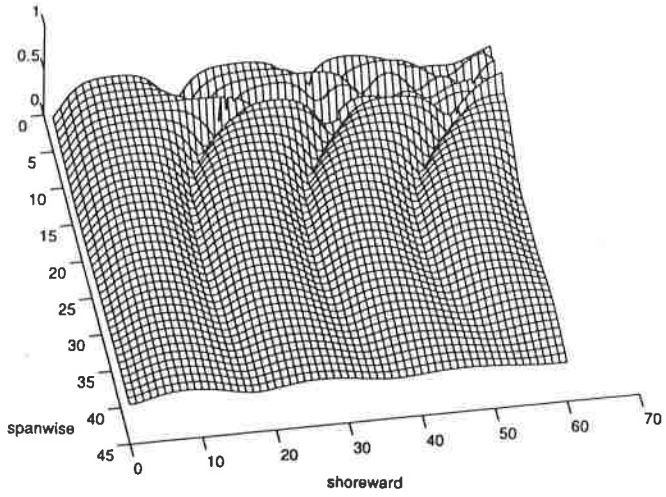

Figure 23. Refraction due to antagonistic boundary conditions and initial bottom configuration. a_2 at $T = 0$.

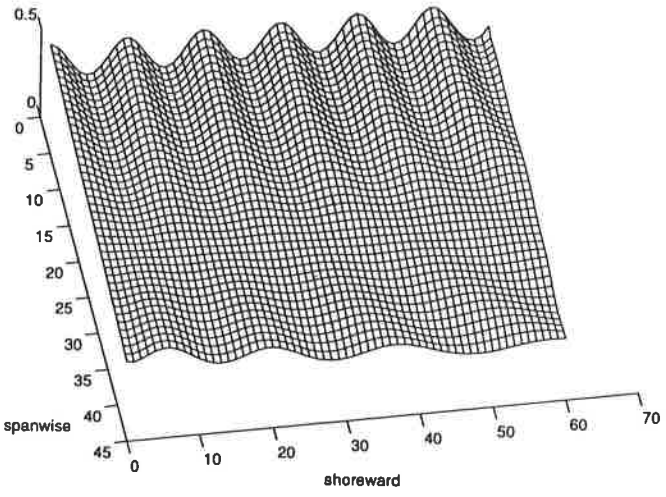

Figure 24. Refraction due to boundary conditions and initial bottom configuration. a_1 at $T = 0$.

5. Conclusions

This study presents the details of a model for the formation and evolution of three-dimensional sedimentary structures on the continental shelf, based on the energetic interactions of weakly nonlinear long waves with the shelf's sedimentary topography. At present, neither the dynamics of sedimentation nor those of water waves are fully understood. If the conjecture is correct, the model will improve in predictive power as understanding of sedimentation and wave dynamics improve. The more important functions played by the model, however, is that its development yields clues to ways in which the conjecture itself may be refined and tested.

The model in its inception was two dimensional. Based on encouraging comparisons with actual field data, the three-dimensional version was developed. Briefly described, the present model couples a mass transport equation, which controls the history of the bottom topography, to a mathematical equation, which describes the evolution of the most energetic wavepackets of surface weakly nonlinear dispersive shallow-water waves with weak spanwise spatial dependence. To solve the coupled system, one relies on the discrepant

time-scales of the bottom evolution and of the water waves to effectively decouple their interaction, making a solution by iteration possible.

The main conjecture of this study is that a significant, but by no means exclusive, agent for the formation and evolution of longshore sand ridges on regions of the continental shelf that are sufficiently removed from the shoaling area is the repeated action of the second-order oscillatory drift velocity that results from the passage of weakly nonlinear dispersive shallow-water waves. If this conjecture is correct, (i) close correlation exists between the interbar spacing and the length in which significant energetic exchanges among the most powerful components of the spectrum of the shallow water waves takes place; (ii) close correlation exists between the evolutionary time-scales for the bars and the time required for highly coherent nonlinear dispersive wave trains to impart sufficient energy into a boundary layer to significantly transform a sediment-laden bottom topography; (iii) longshore sand ridges may be found in areas in which an ample supply of sediment is available and in which no wave breaking occurs and/or in which the reflected field is absent or negligible; (iv) sand ridges with highly organized characteristics may be found in regions in which energetic coherent weakly nonlinear dispersive waves exist; (v) the energy of these waves is of the correct magnitude to significantly affect the topography of a sediment-laden bottom; (vi) the spacing of the bars correlates with the degree of nonlinearity and dispersion of the waves and their orientation is affected proportionally to ξ by the propagation direction of the waves; and (vii) the bottom topography evolves in time-scales measured in T that are much longer than the characteristic times of evolution and adjustment of the water waves, which are in turn measured in t and τ, respectively.

T is really a measure of the time-scales in which changes occur in the wave forcing. In this study we assumed that for infragravity waves, the characteristic time t for their evolution is always shorter than the time T required for appreciable changes to occur in the oceanic forcing. This basic aspect of the model deserves further study. Evidence must be collected in field studies to confirm that the time-scales for the changes in the morphology of the bars are related to the changes in the infragravity forcing. Another basic assumption of the model is that the bars will evolve in a smooth manner unless there are appreciable changes in the oceanic forcing. This also needs to be confirmed in field studies.

Preliminary experimental evidence supports the claim that a relation may exist between the features of the nonlinear long-waves and the bars. Boczar-Karakiewicz *et al* [40],

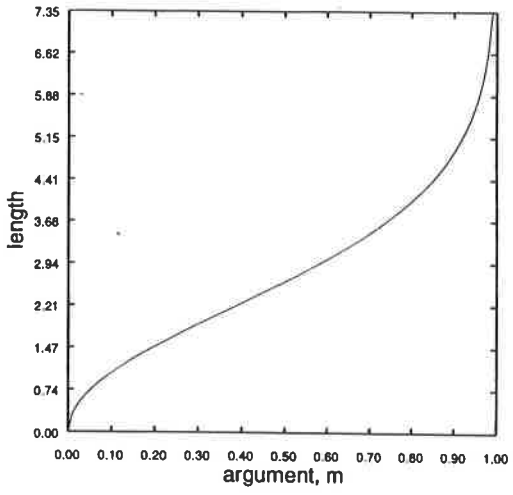

Figure 25. Interaction length dependence on the nonlinear parameter δ. The detuning parameter is scaled so that as $\delta \to 0$, $m \to 1$.

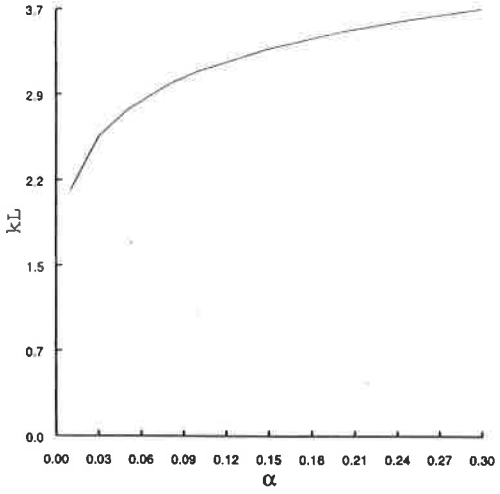

Figure 26. Interaction length dependence on the nonlinear parameter α.

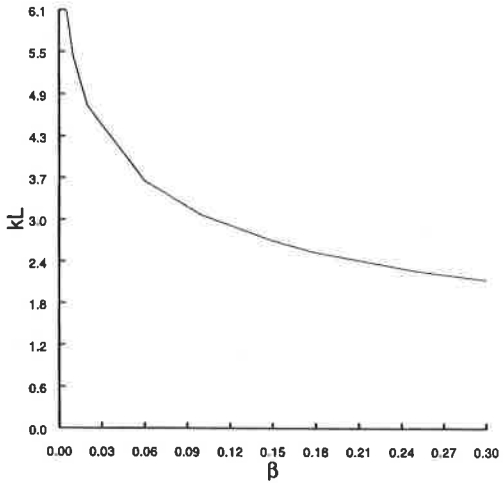

Figure 27. Interaction length dependence on the dispersion parameter β.

in a series of laboratory experiments, observed a relationship between the frequency, the amplitude, and the dispersion, in the waves and the bar spacing. As described in our model, the interaction length is a nonlinear relation that depends on the frequency, the dispersion, and the nonlinearity of the wave. For the two-dimensional case with a flat bottom, the dependence of the interaction length as a function of the detuning parameter is portrayed in figure 25. Figures 26 and 27 illustrate the dependence of the interaction length on the size of the nonlinear parameter α and on the dispersion parameter β. The relevant size of the parameters α and β in the sand ridge case is as high as 0.15 for α and $0.005 < \beta < 0.15$. From the graphs it may be inferred that the interaction length is more sensitive to dispersion than to nonlinearity for the above-mentioned ranges of α and β in qualitative agreement with the aforementioned experiments.

In the future the wavepacket representation of the water waves will be replaced with a better water-wave description. In the mean time, the wavepacket description enables us to determine approximately the dependence of the bar morphology on the variability in spectrum of the infra-gravity forcing. Bona and Saut [63] are studying the different versions of the Boussinesq system in order to determine, among other things, which variant

best models oceanic waves and which is well-posed as a boundary value problem. Another aspect of the model that needs to be studied is the characterization of the net sediment movement, toward the shore or away from it. The net movement is obtained by spatially averaging over the domain the gradient of the drift velocity. In all the time-dependent examples presented in this study, the net movement of the bars was shoreward. This aspect of the model requires determining what characteristics of the infragravity forcing results in net movement toward or away from the shore. An interesting question that has thus far received little attention is the subject of steady-state bottom configurations. In numerical simulations of the present model it has been observed that a common but by no means exclusive long-time outcome for the evolution of the bottom topography is one in which the structure of the wavepacket centres and that of the bottom have similar qualitative features. It is also quite common in these numerical simulations for the bottom to reach its steady state in a gradual fashion rather than in small spurts of high activity followed by relative inactivity, a common observation in the formation of sand ripples [29]. Since little data on the evolution process of actual sand ridges is available it is difficult at present to judge whether the smooth temporal behaviour of the sand ridges created with the present model matches natural bar evolution.

The sensible way to test the model is, of course, to examine oceanic field data. Comparisons with oceanic field data can give an idea of the predictive powers of the model; perhaps laboratory experiments would be most fruitful since the water waves are better characterized and controlled in this setting. The task of making field observations, particularly in the three-dimensional case, is a tedious, expensive, difficult enterprise, and beyond the expertise of the authors.

Several aspects of the model can be tested in the laboratory. First, the drift velocity created by shallow water waves of the type identified here as responsible for the formation of longshore sand ridges could be observed and studied in a laboratory setting in a plume with a fixed bottom, comparisons between the laboratory experiments and the drift velocity measurements in sand ridge fields could prove very fruitful. Second, further experiments aimed at tracking the motion of the sediment in the boundary layer under the action of weakly nonlinear dispersive waves further our understanding of the connection between the wave-generated drift velocity field and the velocity field of the sandy particles. Third, laboratory observations are needed to determine how well the various Boussinesq systems model the weakly nonlinear shallow-water waves.

Field observations are needed to (i) determine the importance of both the reflected wave field and oceanic currents in determining the nature of the drift velocity in sand ridge areas; (ii) correlate in some way the beginning and end of ridge fields and the physical location at which water waves are created and eventually destroyed; (iii) track the relevant wave spectra in order to see evidence of the predicted pattern in energetic interaction lengths and its correlation to features of the bottom topography; (iv) determine what other essential features of the sand ridge formation should be included in this crude model to make it more robust; (v) measure and characterize the boundary layer velocities with the hope of gathering evidence of a periodic structure in the drift velocity that can be correlated in some way to the passing waves; (vi) measure the evolution of the spectra of internal waves in sand ridge evolution time-scales, the aim being to discern how the waves change with morphological changes in the bottom topography; and (vii) (by far the most difficult experiment) the observation of the actual evolution of the bottom topography. If the working assumption is that there may be a variety of agents contributing to the formation and maintenance of sand ridges, we need to thoroughly understand the present model and/or improve upon it with an eye toward developing a clearly verifiable experimental criterion that will enable us to

differentiate this mechanism from any other, since a naive comparison between the present model and field data will contribute little to the validation of the conjectured mechanism. Perhaps the best place to test this model against field data would be in a setting in which ridges are well defined which has an oceanic environment rich in internal interfacial waves. Since interfacial internal waves of the sort relevant to the conjecture are, in some instances, more readily identifiable in the ocean setting than are the surface waves; since they usually develop as strictly progressive waves; and since the place at which they originate, say, a large promontory or the edge of the continental shelf, and the location where the stratification is no longer significant, can be fixed in the ocean setting, the model presented in this study could conceivably be tested with some more confidence.

The geophysics community has expressed some doubts with regard to the role internal waves play in the movement of sediment. Some studies do suggest that the internal waves disappear at times in which significant sediment movement is observed. Beardsley *et al* [64] have shown that in areas off the coast of the eastern United States, the stratification required to support the propagation of internal waves occurs only during summer, a period in which less sedimentary movement has been observed. While data exists that shows a noticeable increase of motion of sandy material during winter storms, these authors do not imply that sediment movement is nonexistent at other times of the year over seasonal time-scales. Furthermore, the appearance of winter storms does not explain the high degree of order in the ridges. The conclusion that sand ridges cannot be formed by internal nonlinear long waves, which may possess energy of the order of hundreds of thousands of watts-minutes, would be correct if it was proven that storms were the only agent for flows strong enough to produce sand movement. The truth is probably that there are many agents for the formation of sand ridges. Among these agents we believe, could be the mechanism presented in this study.

Another issue raised by some geoscientists is that sediment gets entrained most significantly when wave breaking conditions are prevalent. While wave breaking is indeed very effective in lifting sediment off the bottom, it is not a satisfactory explanation for the high degree of order in the bars and does not explain the formation of bars away from the breaking zone.

Finally, in a study by Elgar *et al* [49], it is suggested that the periodic structure of the bars in this model is an artifact of the crude water-wave model based on only a couple of modes. Elgar and his collaborators have examined the issue of the recurrence of solutions to the modally truncated Boussinesq equation numerically in the Stokes parameter regime of O(1). They found that the two-mode case displays recurrence-like solutions over a great many wavelengths. They also found that as the number of modes is increased, the recurrence is confined to fewer and fewer cycles and, further, that initially very narrow spectra undergo more recurrence-like cycles, before the spectra flatten, than do initially broad-banded spectra. Their conclusion is that recurrence-like solutions are an artifact of a severely truncated modal expansion of the Boussinesq equation which, they state, puts doubt on the validity of the conjecture made in this study. They assume, unfortunately, that 'Fermi–Pasta–Ulam recurrence' rather than locally high correlation is a necessary condition for the formation of sand ridges by some forcing action. They also incorrectly assume that their modal formulation for the surface waves and our formulation are analogous. These objections are the subject of a forthcoming paper [58]. For now we remind the reader that the observations of Elgar *et al* do not in any way weaken our conjecture that weakly nonlinear shallow-water waves may be responsible for the formation and evolution of sand ridges, since there is more than ample observational evidence that these nonlinear waves travel coherently over very vast spans of ocean over regions where sand ridges are a prominent

feature of the ocean floor.

While comparisons between field data and the two-dimensional model are very encouraging and this three-dimensional extension should therefore find applicability in the real-world environment, any topographical chart of the continental shelf provides a good reminder of the long path yet to travel toward a complete understanding and model of the full problem. If this study has piqued the curiosity and compelled the reader to take a closer look at sandbars, it will have succeeded.

Acknowledgments

We thank the Applied Research Laboratory at The Pennsylvania State University for making this project possible. This research was supported in part by an appointment to the Distinguished Postdoctoral Research Programme sponsored by the US Department of Energy, Office of University and Science Education Programs, and administered by the Oak Ridge Institute for Science and Education.

References

[1] Davis R A, Fox W T, Hayes M O and Boothroyd J C 1965 Comparison of ridge and runnel systems in tidal and non-tidal environments *Proc. 8th Conf. of Great Lakes Research* (Int. Ass. Great Lakes Research) p 223–31

[2] Off T 1960 Rhythmic sand bodies caused by tidal currents *Bull. Am. Assoc. Petroleum Geologists* **47** 324–341

[3] Allen J R L 1968 *Current Ripples* (Amsterdam: North-Holland) 434

[4] Swift D J P 1968 Quaternary shelves and the return to grade *Marine Geology* **1** 5–30

[5] McBride R A and Moslow T F 1991 Origin, evolution, and distribution of sand ridges, atlantic inner shelf, U.S.A. *Marine Geology* **97** 57–85

[6] Lau J and Travis B 1973 Slowly varying stokes waves and submarine longshore bars *J. Geophys. Res.* **78** 4489–97

[7] Boczar-Karakiewicz B, Amos C L and Drapeau G 1990 The origin and stability of sand ridges on Sable Island bank, Scotian shelf *Continental Shelf Res.* **10** 683–701

[8] Short A 1975 Multiple off-shore bars and standing waves *J. Geophys. Res.* **80** 3838–40

[9] Dean C 1990 Nearshore is plumbed for clues to explain how beach waves act *The New York Times* **C4**

[10] Bijker E W, Hijun E and Vallinga P 1976 Sand transport by waves *Proc. 15th Int. Conf. on Coastal Engineering* p 1149–66

[11] Hallermeier R 1982 Oscillatory bed-load transport *Continental Shelf Res.* **1** 159–90

[12] Elgar S, Guza R T and Freilich M 1988 Eulerian measurements of horizontal accelerations in shoaling gravity waves *J. Geophys. Res.* **93** 9261–9

[13] Sleath J F A 1984 *Sea Bed Mechanics* (New York: Wiley)

[14] Bagnold R A 1963 Motion of waves in shallow water. Interaction of waves and sand bottoms *Proc. R. Soc.* **187** 1–15

[15] Bailard J A and Inman D L 1970 An energetics model for a plane sloping beach. Local transport *J. Geophys. Res.* **75** 5800–12

[16] Smith J D 1970 The stability of a sand bed subjected to shear flow at low Froude numbers *J. Geophys. Res.* **75** 5928–40

[17] Fredœ J 1974 On the development of dunes in erodible channels *J. Fluid Mech.* **64** 1–16

[18] Richards K J Formation of ripples and dunes on an erodible bed *J. Fluid Mech.* **99** 597–618

[19] Dean R 1991 Future directions in cross-shore transport modelling *Coastal Sediment Workshop '91*

[20] Raudkivi A J 1963 Study of sediment ripple formation *Proc. American Society of Civil Engineering, Hydraulics Division* **89** 15–36

[21] Williams P B and Kemp P H 1971 *Proc. American Society of Civil Engineering* **97** 505

[22] Longuett-Higgins M S 1953 Mass transport in water waves *Phil. Trans. R. Soc* **245** 535–81

[23] Stokes G G 1847 On the theory of oscillatory waves *Phil. Trans. R Soc.* **8** 441

[24] Johns B On the mass transport induced by an oscillatory flow in a turbulent boundary layer *J. Fluid Mech.* **70** 177–85

[25] Blondeaux P 1990 Sand ripples under sea waves. Part 1. Ripple formation *J. Fluid Mech.* **218** 1–17

[26] Vittori G and Blondeaux P 1990 Sand ripples under sea waves. Part 2. Finite-amplitude development *J. Fluid Mech.* **218** 19–39
[27] Holman A and Bowen A J 1982 Bars, bumps and holes: model for the generation of complex beach topography *J. Geophys. Res.* **87** 457–68
[28] Bowen A J 1975 On-offshore sand transport on a beach *EOS, Trans. Am. Geophys. Union* (Abstract) **56** 83
[29] Boczar-Karakiewicz B, Benjamin T B and Pritchard W P 1987 Reflection of water waves in a channel with corrugated bed *J. Fluid Mech.* **185** 229–47
[30] Pritchard W G 1990 Personal communication
[31] Mei C C and Ümlüata U 1972 Harmonic generation in shallow water waves *Waves on Beaches* ed R E Meyer (San Diego, CA: Academic)
[32] Hara T and Mei C C 1987 Bragg scattering of surface waves by periodic bars. Theory and experiment *J. Fluid Mech.* **152** 221–41
[33] Mei C C, Hara T and Naciri M 1990 Note on Bragg scattering of water waves by parallel bars on the sea bed *J. Fluid Mech.* **187** 147–62
[34] deVriend H J 1986 2DH computation of transient sea bed evolution *20th Int. Conf. on Coastal Engineering (Taipei)*
[35] Russell R C H and Osorio J D C 1975 An experimental investigation of drift profiles in a closed channel *Proc. 6th. Conf. on Coastal Engineering* p 171–93
[36] Bijker E W, Kalkwijk J P T and Pieters T 1974 Mass transport in gravity waves on a sloping bottom *Proc. 14th Conf. on Coastal Engineering* p 447–65
[37] Huthnance J M 1989 Internal tides and waves near the continental shelf *Geophys. Astrophys. Fluid Dynam.* **48** 81–106
[38] Suhaida J M 1974 Standing waves on beaches *J. Geophys. Res.* **79** 3065–71
[39] Lau J and Barcilon A 1972 Harmonic generation of shallow water waves over topography *J. Phys. Oceanography* 405–10
[40] Boczar-Karakiewicz B, Paplinska B and Winieki J 1981 Formation of sandbars by surface waves in shallow water. Laboratory experiments *Rozprawy Hydrotechnisczne* 111–25
[41] Boczar-Karakiewicz B, Bona J L and Cohen G 1986 Interaction of shallow-water waves and bottom topography, PSU *Applied Mathematics Series* **AM3** Penn State University
[42] Boczar-Karakiewicz B, Bona J L and Pelchat A 1991 Interaction of shallow water internal waves with the bottom topography *Continental Shelf Res.* **11** 234–345
[43] Yang H 1990 Wave packets and their bifurcations in geophysical fluid dynamics *App. Math. Sci.* vol 85 (Berlin: Springer)
[44] Zakharov V E and Shabhat A B Exact theory of two-dimensional self-focusing and one-dimensional self-modulation of waves in nonlinear media *Sov.Phys.–JETP* **34** 62–9
[45] Miles J 1977 On Hamilton's principle for surface waves *J. Fluid Dynam.* **83** 153–8
[46] Bowman S 1986 Hamiltonian formulations and long-wave models for two-fluid systems unpublished
[47] Benjamin T B 1974 Nonlinear Wave Motions (*Lectures on Applied Mathematics* **15**) ed Alan Newell p 3–47
[48] Benjamin T B and Olver P J 1982 Hamiltonian structure, symmetries and conservation laws for water waves *J. Fluid Mech.* **125** 137–85
[49] Elgar S, Freilich M and Guza R T 1991 Recurrence in truncated Boussinesq models of nonlinear waves in shallow water *J. Geophys. Res.* **95** 11 547–56
[50] Lord Rayleigh 1876 On waves *Phil. Mag.* **5** 257–79
[51] Boussinesq J 1871 Theorie de l'intumescence liquid appelee onde solitaire ou de translation, se propagente dans un canal rectangulaire *CR Acad. Sci., Paris* **72** 755–9
[52] Benjamin T B, Bona J L and Mahony J J Model equations for long waves in nonlinear dispersive systems *Phil. Trans. R. Soc.* A **227** 47–78
[53] Kirby J T and Dalrymple R A 1983 A parabolic equation for the combined refraction–diffraction of Stokes waves by mildly varying topography *J. Fluid Mech.* 453–66
[54] Restrepo J M and Bona J L Model for the formation of longshore sand ridges on the continental shelf Mathematics and Computer Science Division, Argonne National Laboratory *Report* MCS-P406-1293
[55] Bona J L 1975 On the stability theory of solitary waves *Proc. R. Soc.* **344** 363–74
[56] Restrepo J M 1992 A model for the formation and evolution of three-dimensional sedimentary structures on the continental shelf *PhD Thesis* The Pennsylvania State University
[57] Druet Cz, Massel S R and Zeidel R 1972 The structure of wind waves in the southern baltic sea *Ruzprawy Hydrotechniczne* **30** 312–8
[58] Restrepo J M, Craig W and McKinney W Modulation equations for shallow water waves, in preparation
[59] Chapalain E 1988 Etude hydrodynamique et sédimentaire des environments littoraux dominés par la houle

Institut de Méchanique de Grenoble, Université de Grenoble *PhD Thesis* 319

[60] Boczar-Karakiewicz B, Forbes D L and Drapeau G 1990 Formation and stability of nearshore bars in the Southern Gulf of St. Lawrence *Geological Survey of Canada* contribution 33 187

[61] Svendsen I A 1977 A model for sedimentary motion under waves *Internal Research Note* Technical University of Denmark, Institute of Hydrodynamics and Hydraulics

[62] Restrepo J M and Bona J L 1993 Discretization of a model for the formation of longshore sand ridges Mathematics and Computer Science Division, Argonne National Laboratory, *Report* MCS-P408-1293

[63] Bona J L Personal communication

[64] Beardsley R C, Chapman David C, Brink K H, Ramp S R and Schlitz R 1985 The Nantucket shoals flux experiment. Part I: a basic despcription of the current and temperature variability *J. Phys. Oceanography* **15** 713–48